1 **Inter-comparison of O_3 formation and radical chemistry in the past decade at a suburban site in**

2 **Hong Kong**

3 Xufei Liu[1,#], Xiaopu Lyu[1,#], Yu Wang[1], Fei Jiang[2], Hai Guo[1,*]

4 [1] Air Quality Studies, Department of Civil and Environmental Engineering, The Hong Kong

5 Polytechnic University, Hong Kong, China

6 [2] Jiangsu Provincial Key Laboratory of Geographic Information Science and Technology,

7 International Institute for Earth System Science, Nanjing University, Nanjing, China

8 *Corresponding author. ceguohai@polyu.edu.hk

9 # Both authors made equal contribution.

10 **Abstract**

11 Hong Kong, as one of the densely populated metropolises in East Asia, has been suffering

12 from severe photochemical smog in the past decades, though the observed nitrogen oxides

13 (NO_x) and total volatile organic compounds (TVOCs) were significantly reduced. This study,

14 based on the observation data in the autumns of 2007, 2013 and 2016, investigated the

15 photochemical ozone (O_3) formation and radical chemistry during the three sampling periods

16 in Hong Kong with the aid of a Photochemical Box Model incorporating the Master

17 Chemical Mechanism (PBM-MCM). While the simulated locally produced O_3 remained

18 unchanged ($p=0.73$) from 2007 to 2013, the observed O_3 increased ($p<0.05$) at a rate of 1.78

19 ppbv/yr driven by the rise in regionally transported O_3 (1.77 $\pm$ 0.04 ppbv/yr). Both the

20 observed and locally produced O_3 decreased ($p<0.05$) from the VOC sampling days in 2013

21 to those in 2016 at a rate of -5.31$\pm$0.07 and -5.52$\pm$0.05 ppbv yr^{-1}, respectively. However, a

22 levelling-off ($p=0.32$) was simulated for the regionally transported O_3 during 2013 – 2016.

23 The mitigation of autumn O_3 pollution in this region was further confirmed by the continuous

24 monitoring data, which has never been reported in previous studies. Benefited from the air

25 pollution control measures taken in Hong Kong, the local O_3 production rate decreased

26 remarkably ($p<0.05$) from 2007 to 2016, along with the lowering of recycling rate of

27 hydroxyl radical (OH). Specifically, VOCs emitted from the source of liquefied petroleum

28 gas (LPG) usage and gasoline evaporation decreased in this decade at a rate of -2.61±0.03

29 ppbv yr^{-1}, leading to a reduction of the O_3 production rate from 0.51±0.11 ppbv h^{-1} in 2007 to

30 0.10±0.02 ppbv h^{-1} in 2016. In addition, solvent usage made decreasing contributions to both

31 VOCs (rate = -2.29±0.03 ppbv yr^{-1}) and local O_3 production rate (1.22±0.17 and 0.14±0.05

32 ppbv h^{-1} in 2007 and 2016, respectively) in the same period. All the rates reported here were

33 for the VOC sampling days in the three sampling campaigns. It is noteworthy that

34 meteorological changes also play important roles in the inter-annual variations of the

35 observed O_3 and the simulated O_3 production rates. Evaluations with more data in longer

36 periods are therefore recommended. The analyses on the decadal changes of the local and

37 regional photochemistry in Hong Kong in this study may be a reference for combating

38 China's national-wide O_3 pollution in near future.

39 **Keywords:** Ozone formation; Volatile organic compounds; Radical chemistry; Source

40 apportionment; Control measures

41 **1 Introduction**

42 Ground-level ozone (O_3) is one of the most representative air pollutants in photochemical

43 smog, produced through photochemical reactions between volatile organic compounds

44 (VOCs) and nitrogen oxides (NO_x) in presence of sunlight (NRC, 1992; Jacob et al., 1999;

45 Guo et al., 2017). It is well documented that O_3 is harmful to human health (Bell et al., 2004),

46 crops (Wang et al., 2005) and natural ecosystems (Ashmore, 2005). Through the last 30 years,

47 extensive efforts have been made by the local and federal governments to alleviate the

48 tropospheric O_3 pollution around the world (NRC, 1992; NARSTO, 2000; Wang et al., 2017a;

49 Wang et al., 2018a). Effectiveness has gradually shown in some countries/regions, such as

50   Switzerland, Germany, Ireland and eastern North America (Lefohn et al., 2010; Cui et al.,

51   2011; Derwent et al., 2013; Parrish et al., 2014; Lin et al., 2017). In contrast, the O_3 levels in

52   many places are still increasing or not decreasing at the expected rates, particularly in East

53   Asia (Ding et al., 2008; Xu et al., 2008; Parrish et al., 2014; Xue et al., 2014a; Wang et al.,

54   2017a).

55   Hong Kong, as one of the densely populated metropolises in East Asia, has been suffering

56   from severe photochemical smog in the past decades, though the locally-emitted NO_x and

57   total VOCs (TVOCs) were significantly reduced (Xue et al., 2014a; Ou et al., 2015; Lyu et al.,

58   2016a; Wang et al., 2017a). On one hand, this indicates the non-linear relationship between

59   O_3 and its precursors. On the other hand, in addition to local O_3 formation, the observed O_3 in

60   Hong Kong is also influenced by the regional transport due to the proximity of the highly

61   industrialized Pearl River Delta (PRD) region. Earlier studies revealed that the local O_3

62   production is typically limited by VOCs in urban and some suburban areas in Hong Kong

63   (Zhang et al., 2007; Ling et al., 2014; Wang et al., 2017b). Namely, cutting VOCs emissions

64   will reduce O_3 production, while the reduction of NO_x may cause an O_3 increment (Cheng et

65   al., 2010, 2013; Guo et al., 2011; Wang et al., 2017a). Previous studies also documented that

66   photochemical O_3 formation is dependent upon the ratios between TVOCs and NO_x (Sillman,

67   1999; Guo et al., 2013a; Ling et al., 2013), reactivity of VOC species (Zhang et al., 2007; Liu

68   et al., 2008; Cheng et al., 2010) and the composition of NO_x (*i.e.* relative abundances of NO_2

69   and NO) (Richter et al., 2005; Xu et al., 2008; Wang et al., 2018a). Moreover, located in the

70   subtropical region, Hong Kong has relatively high temperature and strong solar radiation,

71   which are favourable for local O_3 formation. For regional transport, studies (Wang et al.,

72   2001; Ding et al., 2004; Wang et al., 2017b) indicated that O_3 was generally built up in Hong

73   Kong under the northerly winds, whereas it was often driven down by the sea breeze from

74   South China Sea (SCS) and by the southwest monsoon in warm seasons. The contribution of

75 regional transport to O_3 in Hong Kong even reached 70% under the dominance of tropical

76 cyclone (Huang et al., 2005), a typical synoptic condition conducive to severe O_3 pollution in

77 the Northern Hemisphere (So and Wang, 2003; Huang et al., 2005; Lam et al., 2005). To

78 improve the air quality in Hong Kong, a series of control measures aiming at restriction of

79 VOC emissions have been implemented by Hong Kong government since 2007, which

80 effectively reduced the concentrations of some VOCs, such as propane and *i-/n*-butanes

81 emitted from taxis and public light buses fuelled by liquefied petroleum gas (LPG) (Lyu et al.,

82 2016b), the aromatics mainly attributable to solvent usage, and the alkenes in association

83 with diesel exhaust (Lyu et al., 2017a). As a result, Xue et al. (2014a) and Wang et al.

84 (2017a) found that the locally produced O_3 decreased. However, the regional and super-

85 regional transport of O_3 and its precursors from PRD and eastern China to Hong Kong had

86 offset the decrease of the local O_3 production, resulting in an overall increase of the observed

87 O_3 in Hong Kong from 2005 to 2013. Overall, the previous studies have greatly enhanced our

88 understanding on O_3 pollution in Hong Kong, and details about the studies can be referred to

89 in Table S1.

90 Despite many previous studies (Xue et al., 2014a, 2016; Ou et al., 2015; Lyu et al., 2016a;

91 Wang et al., 2017a; Wang et al., 2018a), the inter-annual variations of the O_3 formation

92 regimes and radical chemistry have yet been fully understood in Hong Kong. Additionally,

93 the online measurement data used in previous long-term O_3 study might hamper the exact

94 understanding of the local O_3 formation mechanisms, due to the unavailability of many

95 reactive VOCs, such as formaldehyde. Besides, the trends of the local production and

96 regional transport of O_3 were only updated to 2013 in previous studies (Xue et al., 2014a;

97 Wang et al., 2017a). In fact, many measures were taken to reduce air pollutants' emissions in

98 the latest years in Hong Kong and PRD. For examples, nearly 75% of the old catalytic

99 converters on LPG-fuelled vehicles were renewed during September 2013 - May 2014. A

100   program to eliminate the pre-Euro IV diesel vehicles or to upgrade their emission standards to

101   Euro IV was initiated in March 2014 and is still ongoing till 2019 at its third phase. In PRD,

102   the second stage of the clean air controlling program was implemented in 2013 - 2015

103   (DGEPD, 2013). In 2014, the Guangdong provincial government has launched an Action

104   Plan for Air Pollution Prevention and Control (MEE PRC, 2014), putting the emphases on the

105   emission control of traffics, coal-fired power plants and industrial sources. Investigations on

106   the post-2013 variations of the local O_3 production in Hong Kong and the regional impacts

107   provide a good opportunity for us to examine the effectiveness of these local and regional

108   measures.

109   The objectives of this study were to re-examine the O_3 trend in the pre-2013 and trace the O_3

110   evolution in the post-2013 in Hong Kong, and to explore the underlying mechanisms for the

111   variations of O_3 formation and radical chemistry. With the aid of a photochemical box model,

112   the locally produced and regionally transported O_3, as well as their variation trends, were

113   determined (see section 2.5). Under the assumption that the local O_3 production in these years

114   was changed due to a series of control measures in Hong Kong, we also aimed to evaluate the

115   actual effectiveness of these control measures. China is suffering from severe O_3 pollution,

116   almost second to none over the world. While O_3 began to decrease in most areas of North

117   America and Europe, China's O_3 pollution was even aggravated in recent years. A series of

118   air pollution control strategies have been implemented in China, though most of them were

119   not specifically designed for O_3 abatement. Investigations on O_3 trends and the potential

120   causes in Hong Kong would provide a good example of assessing the evolution of O_3

121   pollution and the effects of artificial interventions in China. In addition, the changes in the

122   regional contribution to O_3 in Hong Kong determined in this study would throw light upon

123   the variations of O_3 in China, particularly in South China. It is expected that this study would

124   have some inspiration to the O_3 pollution control in other cities and regions in China.

2 Methodolgy

2.1 Sampling site

Hong Kong is located on the southern coast of China with Guangdong province to the north and Pearl River Estuary (PRE) to the northwest. The sampling site (22.29N, 113.94E), Tung Chung (TC), was in a newly-developed suburban area in western Hong Kong, with a population of ~77,400 in 2016 (CSD, 2011, 2018). The urban centre of Hong Kong is ~20 km northeast of TC. Hong Kong is dominated by the subtropical oceanic monsoon climate. During warm seasons, the prevailing winds mainly come from SCS at a relatively low speed (southwest winds). In cold seasons, the east and northeast winds are predominant. Generally, the sampling site receives relatively polluted air masses from mainland China, *i.e.* PRD region, Yangtze River Delta region and even North China between October and March, when high O_3 levels are often observed (Wang et al., 2009). Therefore, the samplings were mainly conducted in October and November in this study, except for 4 out of 45 sampling days in September. The sampling site was close to a highway linking to the Hong Kong International Airport (HKIA), and the HKIA was around 3 km to the north of the site. In addition, the local emissions from residential activities may modulate the air quality at this site. It was expected that O_3 at TC would be significantly influenced by NO emitted from the aforementioned sources. As shown in Figure S1, the O_3 titrated by NO ($\triangle O_3$-1) was equivalent to 29.9±8.8%, 26.7±12.7% and 32.5±16.6% of the photochemically formed O_3 ($\triangle O_3$-2) in the 2007, 2013 and 2016 sampling campaigns, respectively, confirming the importance of NO titration in modulating O_3 at the site. Figure 1 shows the locations of the sampling site (TC) and the 12 air quality monitoring stations in PRD, which witnessed the evolution of air quality in PRD over the last decade and is used to demonstrate the variations of regional O_3 in this study. More detailed description of the site can be found in our previous studies (Jiang et al., 2010: Cheng et al., 2010; Ling et al., 2013; Ou et al., 2015).

150
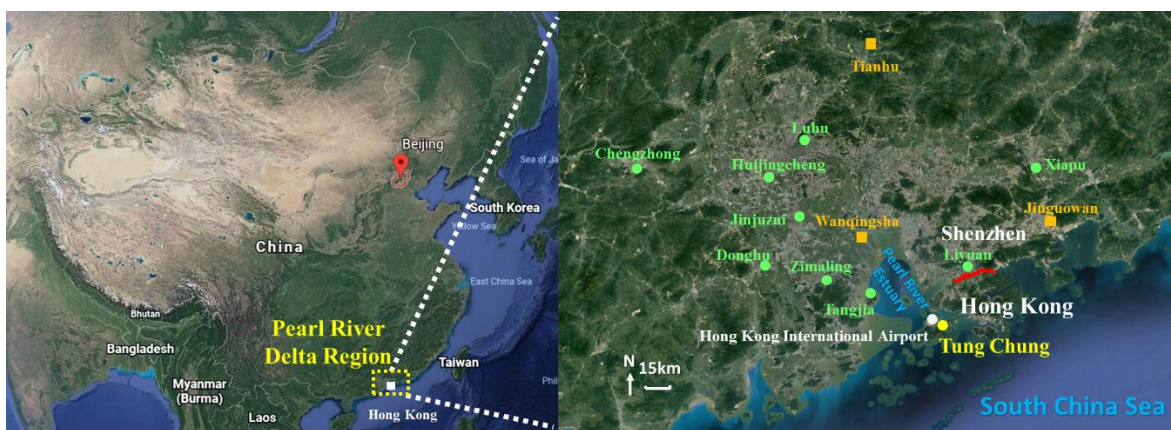
Figure 1. Location of the sampling site (yellow circle) and the surrounding environment. The red line in the right panel shows the border between Hong Kong and Shenzhen, Guangdong. The three regional and nine urban air quality monitoring stations in PRD are symbolized by orange blocks and green circles, respectively.

2.2 Continuous measurements of trace gases and collection of VOC/OVOC samples

Trace gases (SO_2, CO, NO, NO_2 and O_3) and meteorological conditions were continuously measured at TC site for three autumn periods in 2007, 2013 and 2016 (see Table S2 for the specific sampling periods), including 25 O_3 episode days with the maximum hourly average O_3 exceeding 100 ppbv (Level II of China National Ambient Air Quality Standard) and 185 non-episode days. VOC and OVOC samples were selectively collected on 8, 19 and 18 days in 2007, 2013 and 2016, respectively (see Table S2 for the specific sampling dates). The three sampling periods were used as representatives of the autumns in the three years in this study, and the rationality will be discussed in section 3.1.

Trace gases were continuously measured at the TC air quality monitoring station operated by the Hong Kong Environmental Protection Department (HKEPD), ~0.8 km to our sampling site. The instruments were the same as those used in the US air quality monitoring program (HKEPD, 2017a). Table S3 summarizes the instruments, analysis techniques, detection limits and the time resolutions for measurements of the trace gases. The high resolution data were

7

collected and averaged into the hourly averages. All the analysers except O_3 analyser were zeroed daily by analysing scrubbed ambient air and calibrated every two weeks by a span gas mixture with a NIST (National Institue of Standards and Technology) traceable standard, while the O_3 analyser was calibrated using a transfer standard (Thermo Environmental Instruments (TEI) 49PS) every two weeks. Details about the quality assurance and control procedures can be found in Ling et al. (2016a). The meteorological parameters, including temperature, relative humidity, pressure, wind speed, wind direction, precipitation and solar radiation, were also continuously monitored by a mini weather station (Vantage Pro TM & Vantage Pro 2 Plus TM Weather Stations, Davis Instruments) during the sampling periods. Data were integrated into 30-minute averages by a built-in program in the weather station. The collection and analysis of VOCs and OVOCs were detailed in our previous studies (Guo et al., 2009; Wang et al., 2018b). Briefly, pre-cleaned and evacuated 2 L electropolished stainless-steel canisters were used to collect VOC samples. On O_3 episode days, one-hour sample was collected in each hour during the daytime (07:00-19:00 LT), generating 13 samples per day, while 5-7 one-hour samples were collected every other hour on non-O_3 episode days from 07:00 to 19:00 LT in the 2013 and 2016 sampling campaigns. However, 12 one-hour samples were collected on each VOC sampling day between 07:00 and 18:00 in 2007, regardless of O_3 episodes or non-episodes. The O_3 episode days were predicted prior to sampling based on weather forecast and numerical simulation of O_3. Overall, the O_3 episodes were usually associated with high temperature, strong solar radiation, low humidity, and weak or northerly winds. A total of 414 canister samples, including 96 samples in 2007, 146 samples in 2013 and 172 samples in 2016, were collected and analysed during the three sampling periods (Table S2).

In addition to VOC samples, OVOC samples were also collected on the same days as those for the collection of VOCs. Dinitrophenylhydrazine (DNPH)-silica cartridges (Waters Sep-

194   Pak DNPH-Silica, Milford, MA) were used to collect the OVOC samples. An ozone scrubber

195   (Sep-Pak; Waters Corporation, Milford, MA) was connected in front of the DNPH cartridge

196   to prevent interference of ozone. The ozone scrubber was replaced every two OVOC samples.

197   For each OVOC sample, air was drawn to pass the O_3 scrubber and the cartridge for 2 hours

198   (2.5 hours in 2007 sampling campaign) at a flow rate of 0.5 L min^{-1}, which was controlled by

199   a rotameter. During the sampling periods in 2013 and 2016, 5-7 OVOC samples were

200   collected every two hours from 06:00-20:00 LT on both O_3 episode and non-episode days. In

201   2007, only 2 samples were collected on non-O_3 episode days at 10:30-13:00 and 13:00-15:30,

202   and 4 samples between 08:00 and 18:00 on O_3 episode days. In total, 275 OVOC samples (28

203   in 2007, 124 in 2013 and 124 in 2016) were collected and analysed in the three sampling

204   campaigns (Table S2).

205   **2.3 Chemical analysis**

206   2.3.1 Analysis of VOCs

207   The concentrations of 48 speciated non-methane hydrocarbons (NMHCs) in the canisters

208   were determined with an Entech Model 7100 Preconcentrator (Entech Instruments Inc.,

209   California, USA) coupling with a gas chromatography-mass selective detector (Model 5973N,

210   Agilent Technologies, USA), a flame ionization detector, and an electron capture detector

211   (GC-MSD/FID/ECD). The NMHCs were analysed in Guangzhou Institute of Geochemistry

212   (GIG), Chinese Academy of Sciences for the samples collected in both 2007 and 2013, and in

213   The Hong Kong Polytechnic University (HKPolyU) for the samples collected in 2016. It

214   should be noted that the GC-MSD/FID/ECD system in the latter two institutes was the same

215   as that at UCI, and inter-comparisons were performed regularly among the three institutes,

216   which showed reasonably good agreements (Ling et al., 2014; Wang et al., 2018b; Zeng et al.,

217   2018). Detailed information about the analysis procedures and quality assurance and control

218   can be found in Colman et al. (2001) and Simpson et al. (2010). Table S4 summarizes the

219   limits of detection (LoDs), precisions and accuracies of the VOC analyses in the three

220   institutes.

221   The OVOC samples were stored in a refrigerator at 4°C after sampling. For analyses of

222   OVOCs, the cartridges were eluted slowly with 2 ml of acetonitrile into a 2-ml volumetric

223   flask. A high-performance liquid chromatography (HPLC) system (Perkin Elmer Series 2000,

224   MA, USA) coupled with an ultraviolet (UV) detector operating at 360 nm was used for

225   analysis. The instrument was calibrated using standards of 5 gradient concentrations covering

226   the concentrations of interest for different OVOCs in ambient air. Good linear relationships

227   ($R^2 > 0.999$) between the standard concentrations and responses of the instrument were

228   obtained for the 16 analysed OVOC species. The built-in computerized programs of quality

229   control systems such as auto-linearization and auto-calibration were used to guarantee the

230   data quality. Detailed information about the analysis and quality control of OVOC samples

231   was provided in Cheng et al. (2014), Cui et al. (2016) and Ling et al. (2016b). Due to the low

232   detection rate of many OVOCs, this study only focused on formaldehyde, acetaldehyde,

233   acetone and propionaldehyde, which had relatively high concentrations.

234   **2.4 Model description**

235   **2.4.1 Positive matrix factorization (PMF)**

236   PMF is a receptor model that has been extensively used for source apportionment of airborne

237   particulate matters and VOCs (Lee et al., 1999; Brown et al., 2007). In this study, US EPA

238   PMF 5.0 model (US EPA, 2017) was applied to identify the sources of O_3 precursors,

239   according to Equation (1) (Paatero, 1997; Ling et al., 2014).

240   $$x_{ij} = \sum_{k=1}^{p} g_{ik} f_{kj} + e_{ij}$$ Equation (1)

241   where x_{ij} is the measured concentration of jth species in ith sample, g_{ik} represents the

242   contribution of kth source to ith sample, f_{kj} denotes the fraction of jth species in kth source,

243   and e_{ij} is the residual for jth species in ith sample. p stands for the total number of

244   independent sources (Paatero, 2000a, b).

245   The uncertainties of the concentrations applied to PMF were set in the same way as Polissar

246   et al. (1998) and Reff et al. (2007). Values below or equal to the LoD were replaced by half

247   of the LoDs and the uncertainties for these values were set as 5/6 of the corresponding LoDs.

248   For the values greater than LoDs, the uncertainties were calculated as [(Error Fraction $\times$

249   concentration)^2 + (LoD)^2]$^{1/2}$ where 10% was assigned as the error fraction. Missing values

250   (mainly due to maintenance or malfunction of the instruments) were replaced by the

251   geometric mean of the measured values and their accompanying uncertainties were set as

252   four times the geometric mean value. More details about the settings of the uncertainty were

253   provided in Norris et al. (2008) and Zhang et al. (2012).

254   The model was run for 20 times with a random seed, and tests with different number of

255   factors were conducted. The optimum solution was finally determined based on both a good

256   fit to the observed data and the most reasonable and interpretable results according to the

257   knowledge on the sources of O_3 precursors in Hong Kong (Ling et al., 2011, 2014; Ou et al.,

258   2015).

259   **2.4.2 Observation-based model (OBM)**

260   A photochemical box model coupled with the Master Chemical Mechanism (PBM-MCM)

261   was used to simulate the photochemical O_3 formation on the VOC sampling days. In this

262   study, MCM v3.2, a near explicit chemical mechanism consisting of 5,900 species and

263   16,500 reactions which fully describes the homogeneous gas phase reactions in the

264   atmosphere (Jenkin et al., 1997, 2003; Saunders et al., 2003), was used. The observation data

265 of temperature, relative humidity, O_3, SO_2, CO, NO, NO_2 and 52 C_2-C_{10} VOCs/OVOCs were

266 input into the model. Specifically, the 52 VOCs/OVOCs included 19 alkanes, 16 alkenes, 13

267 aromatics and 4 OVOCs, as shown in Table S5, where the statistics of the mixing ratios of

268 VOCs/OVOCs are also presented. Though previous studies (Guo et al., 2013b; Ling et al.,

269 2016b) indicated that secondary formation dominated the sources of OVOCs in Hong Kong,

270 the primary emissions could not be neglected. Therefore, formaldehyde, acetaldehyde,

271 acetone and propionaldehyde with relatively high abundances were constrained to the

272 observed concentrations in the model, while the other OVOCs with low concentrations and

273 low detection rates were simulated by the model. Nitrous acid (HONO) was not monitored in

274 this study. The average diurnal cycle of HONO mixing ratios measured at the same site in

275 autumn in 2011 (Xu et al., 2015) was input into the model to roughly represent its role in O_3

276 formation and atmospheric radical chemistry. Due to the data limitation, the trends of HONO

277 at TC in the three sampling campaigns were not traceable. However, the measurements at a

278 background site in Hong Kong indicated comparable levels of HONO (p>0.1) between the

279 autumn in 2012 and in 2018 (unpublished data). Therefore, adopting the HONO measured in

280 2011 as the inputs of the simulations in the three sampling campaigns was likely a plausible

281 assumption, despite some uncertainties. The model was also tailored to the real situations in

282 Hong Kong. Specifically, the height of the planetary boundary layer was allowed to vary

283 from 300 m at night to 1400 m at noon. The photolysis rates were calculated according to the

284 measured solar radiations by the Tropospheric Ultraviolet and Visible Radiation model

285 (Madronich and Flocke, 1999; Wang et al., 2017a), with the detailed method described in

286 Lyu et al. (2017b). In addition to the chemical processes, the exchange between the lower

287 troposphere and free troposphere, and dry deposition were also considered in the model. The

288 concentrations of air pollutants in the free troposphere were set according to the observations

289 at a mountainous site in Hong Kong (Lam et al., 2013). The dry deposition rates were

290 adopted from the previous studies (Saunders et al., 2003; Lam et al., 2013). The other

291 physical processes were not included in the model, which might lead to insufficient

292 description of the transport. However, since the model was constrained to the observations

293 which included the transported air pollutants, the regional transport was partially considered.

294 Besides, the observations at 07:00 on each day were used to initiate each day's modelling,

295 through which the effect of regional transport before the daytime modelling was also

296 considered. We admit that the PBM-MCM cannot perfectly reproduce the real atmospheric

297 processes. However, it performed well in describing the in-situ photochemistry in previous

298 studies (Lam et al., 2013; Ling et al., 2014; Lyu et al., 2017b; Wang et al., 2017a). Actually,

299 the deficiency of PBM-MCM in consideration of the atmospheric dynamics enabled us to

300 assess the contributions of regional transport to O_3 in Hong Kong, based on the differences

301 between the observed and simulated O_3 (Wang et al., 2017a).

302 **2.5 Simulation scenarios**

303 The PBM-MCM simulates the in-situ O_3 photochemistry based on the observed O_3 precursors.

304 Figure S2 shows the average mixing ratios of some O_3 precursors in different wind sectors.

305 The higher levels of CO, ethyne, ethane, propane and toluene under northwest winds

306 indicated the transport of these species from PRD to Hong Kong. Meanwhile, O_3 might also

307 be transported to Hong Kong. Text S1 discusses the determination of the locally produced

308 and regionally transported O_3, as well as the uncertainties. Furthermore, to evaluate the

309 contributions of VOC sources to the local O_3 production, two scenarios of model simulation

310 were performed, *i.e.,* Scenario A and Scenario B. The scenario A simulated the O_3

311 photochemistry in the whole air, which was constrained by the observed concentrations of all

312 the O_3 precursors. The model simulations in scenario B (including six assumed sub-scenarios)

313 were constrained by the concentrations of O_3 precursors with those contributed by individual

314 sources being subtracted from the observed concentrations. Text S2 elaborates the set-up of

13

315   these scenarios. The simulated O_3 in scenario A was regarded as the locally produced O_3, as

316   the observed O_3 concentrations were not input to constrain the model. Bearing in mind that

317   the regional effects cannot be completely eliminated in this approach, due to the impacts of

318   regional air on the observed concentrations of O_3 precursors. The differences between the

319   scenario A and scenarios B reflected the contributions of the individual sources to the

320   simulated O_3 production rate. It should be noted that due to the nonlinear relationships

321   between O_3 and its precursors, the subtraction approach only qualitatively rather than

322   quantitatively evaluated the contributions of VOC sources to O_3 production.

323   **3 Results and discussion**

324   **3.1 Observation overview**

325   Figure 2 shows the hourly mixing ratios of O_3 observed at TC in the autumns of 2007-2017

326   with the data on VOC sampling days being highlighted in red. It was found that the autumn

327   O_3 increased significantly from 2007 to 2013 ($p<0.01$), with a rate of 0.34 ± 0.002 ppbv yr^{-1}.

328   This was consistent with Wang et al. (2017a) who reported an overall increase rate of autumn

329   O_3 of 0.67 ± 0.07 ppbv yr^{-1} at the same site for the period of 2005-2013. On one hand, the

330   discrepancy in O_3 increasing rates might be due to the different statistics used to draw the

331   rates, *i.e.* hourly values in this study and monthly averages in Wang et al. (2017a). On the

332   other hand, the autumn O_3 increased substantially from 23.9 ± 0.97 ppbv in 2005 to 30.2 ± 0.97

333   ppbv in 2007, much quicker than the increase between 2007 and 2013. Without the inclusion

334   of the period of 2005-2007 might be another reason of the less O_3 enhancement calculated

335   here. In contrast to the increased autumn O_3 during 2007-2013, the autumn O_3 decreased

336   obviously from 2013 to 2017 ($p<0.01$), at a rate of -2.27 ± 0.003 ppbv yr^{-1}, indicating a

337   fundamental alleviation of O_3 pollution in Hong Kong in the latest 5 years. Overall, a

338   statistically significant decreasing trend (rate = -0.44 ± 0.001 ppbv yr^{-1}) was observed for the

339   autumn O_3 at TC through 2007 to 2017 ($p<0.05$). The average O_3 on VOC sampling days in

340 the three sampling campaigns also followed the same pattern, which increased from

341 32.8±2.6 ppbv in 2007 to 36.9±2.3 ppbv in 2013, while decreased to 24.4±1.9 ppbv in 2016.

342 Further, we investigated the number of O_3 episode days in the autumns of the three VOC

343 sampling years (see Figure S3) and identified 15 (16.5% of the autumn days, same below)

344 and 16 (17.6%) O_3 episode days in 2007 and 2013, respectively. However, there was only 5

345 (5.5%) O_3 episode days in the autumn of 2016. Similarly, the O_3 episode days accounted for

346 12.5%, 26.3% and 5.6% of the 2007, 2013 and 2016 sampling campaigns, respectively.

347 Therefore, the increase of O_3 from 2007 to 2013 and the decrease in the following years

348 could be represented by O_3 observed in the three sampling periods.
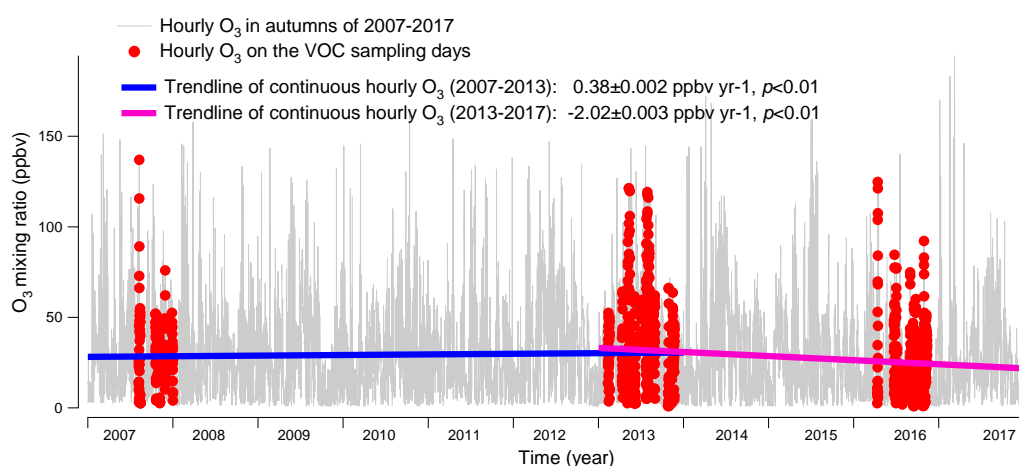
349

350 Figure 2. Long-term trends of the observed O_3 at TC from 2007 to 2017. Hourly O_3 values on
351 the VOC sampling days in the autumns of 2007, 2013 and 2016 are marked in red. The
352 hourly variation rates of O_3 are converted to yearly rates in periods of 2007 – 2013 and 2013
353 – 2017.

354 Table 1 and Table S6 present the observed O_3, CO, NO, NO_2, SO_2 and TVOCs, as well as the

355 meteorological conditions averaged on the VOC sampling days in 2007, 2013 and 2016,

356 respectively. From 2007 to 2013, the TVOCs decreased by nearly a half, which was expected

357 to result in the reduction of O_3 in view of the VOC-limited regime of O_3 formation at TC

358 (Cheng et al., 2010; Wang et al., 2017a). However, the increases of CO and the notable

15

359   decrease of NO in 2013 could enhance the O_3 production. The higher O_3 in 2013 indicated

360   that this effect overrode the reduction of TVOCs in influencing the O_3 production. In

361   particular, the decrease of NO meant the reduced NO titration to O_3, which has been

362   recognized as a primary reason of O_3 increase in VOC-limited regime (Chou et al., 2006;

363   Wang et al., 2018b). From 2013 to 2016, the decrease of O_3 was accompanied by the

364   reductions of TVOCs and NO_2, though CO remained increasing at the same time. NO_2, as a

365   direct source of O_3 through photolysis, plays important role in modulating the O_3 variation.

366   Though the causes of NO_2 reduction are unknown to us, it might be one of the critical factors

367   contributing to the decline of O_3 in Hong Kong in recent years. On the contrary, the increase

368   of CO was also confirmed by the continuous monitoring data at TC, with a rate of

369   33.9 ± 0.7 ppbv yr^{-1} between 2013 and 2016. In fact, the consistent increasing trend ($p<0.05$)

370   was also observed at the roadside sites in Hong Kong (not shown here). While the causes of

371   CO increase in Hong Kong may be complicated, the increased vehicle emission is a plausible

372   explanation. Studies (Johnson, 2008; Yao et al., 2008) revealed that while the new engine

373   technologies performed well in reducing NO_x emission, they might lead to the increased

374   emission of CO, with the application of lower air-to-fuel ratio and engine temperature.

375   In addition, studies have confirmed that continental anticyclones and tropical cyclones are

376   conducive to severe O_3 pollution in Hong Kong, because these synoptic systems are often

377   accompanied with northerly winds, high temperature, strong solar radiation, and relatively

378   high pressure in Hong Kong (Ding et al., 2004; Huang et al., 2005; Jiang et al., 2015).

379   Table S7 summarizes number of O_3 episode days with tropical cyclone, continental

380   anticyclone and low pressure trough in the autumns of 2007, 2013 and 2016. In autumn 2007,

381   8, 8 and 1 O_3 episode day(s) were found to be related to the tropical cyclone, continental

382   anticyclone and low-pressure trough, respectively, with 2 O_3 episode days under the

383   combined influence of tropical cyclone and continental anticyclone. There were also 11 and 5

16

384 O$_3$ episode days in association with tropical cyclone and continental anticyclone in autumn

385 2013, respectively (Wang et al., 2018b). However, 4 out of the 5 episode days found in

386 autumn 2016 were associated with tropical cyclone, with the other one related to low-

387 pressure trough. Therefore, the lower O$_3$ and less O$_3$ episode days in 2016 were also benefited

388 from the meteorological conditions.

389 Table 1. Mixing ratios of the measured trace gases and TVOCs averaged on the selective 45

390 VOC sampling days in 2007, 2013 and 2016.

	2007		**2013**		**2016**	
Unit: ppbv	Mean ± 95% C.I.	Max.	Mean ± 95% C.I.	Max.	Mean ± 95% C.I.	Max.
O$_3$	32.8±2.6	137.0	36.9±2.2	121.2	24.4±1.9	124.9
CO	456.3±19.8	847.0	585.0±11.9	1047.9	691.8±9.5	1074.7
NO	17.2±3.2	124.7	10.9±1.3	98.6	11.3±1.4	94.6
NO$_2$	27.7±2.1	69.6	31.5±1.4	80.8	22.0±1.1	103.2
SO$_2$	6.9±0.4	21.8	7.0±0.2	18.0	3.0±0.1	10.7
TVOCs	49.7±4.4	111.1	25.1±1.4	68.0	21.1±1.4	71.9

391

3.2 Model simulation of O$_3$

3.2.1 Model validation

394 Figure 3 compares the simulated O$_3$ in scenario A and the observed O$_3$ on the VOC sampling

395 days. Overall, both the magnitudes and the temporal patterns of the observed O$_3$ were

396 reasonably reproduced, though the mean of the simulated O$_3$ (33.8±1.9 ppbv) was slightly

397 lower than the observed average (37.1±2.0 ppbv). To quantitatively evaluate the model

398 performance, the index of agreement (IOA) was used to examine the goodness of fit between

399 simulated and observed O$_3$. Within the range of 0-1, higher IOA represents better agreement

400   between the simulated and observed values (Willmott, 1982). In this study, the overall IOA

401   for the three sampling periods was 0.74, within the range of IOA (0.67-0.89) accepted by the

402   previous studies (Wang et al., 2015; Lyu et al., 2015, 2016a, c; Wang et al., 2017a, 2018a).

403   Good correlations (R^2=0.61) were also shown between the simulated and observed hourly O_3.

404   Bearing in mind the deficiencies of the box model in describing the atmospheric dynamics,

405   we believed that the modelling results were acceptable, but special attention and explanation

406   to the discrepancies between the simulated and observed O_3 was needed.

407   It was found that the discrepancies were most likely caused by the transport processes, *i.e.,*

408   vertical and horizontal transport, which were not fully represented in the PBM-MCM model

409   (George et al., 2013; Lakey et al., 2015; Wang et al., 2017a). For example, the simulated O_3

410   (maximum: 122.6 ppbv) was much higher than the observed O_3 (maximum: 44.3 ppbv) on

411   November 16, 2007, when the strong southeast winds (wind direction: 90°-180°) with the

412   highest wind speed of 5.3 m s^{-1} prevailed in Hong Kong. The south sector winds from SCS

413   might dilute the locally produced O_3 and the O_3 precursors/intermediates (such as the radicals)

414   which were not constrained by the observations. The same circumstances were also observed

415   on October 27, November 17, 2007 and September 11-12, November 20, 2013, with

416   southeast winds dominated (74.4%) during the daytime (Figure 3). For those days with the

417   simulated O_3 lower than the observed O_3, *i.e.* October 3, 22-25, 2013 and November 6, 2016,

418   69.3% of the winds during the daytime came from the north (wind directions: 0-90° and

419   270°-360°), which might transport the air masses laden with O_3 and/or O_3

420   precursors/intermediates not constrained to the observations from inland PRD to the sampling

421   site. The observed O_3 mixing ratios are plotted against the wind fields in Figure S4. It is

422   obvious that O_3 were higher under the north winds, while lower in the south wind sectors,

423   confirming the effects of dilution and regional transport of the south and north winds on O_3

424   pollution in Hong Kong, respectively.
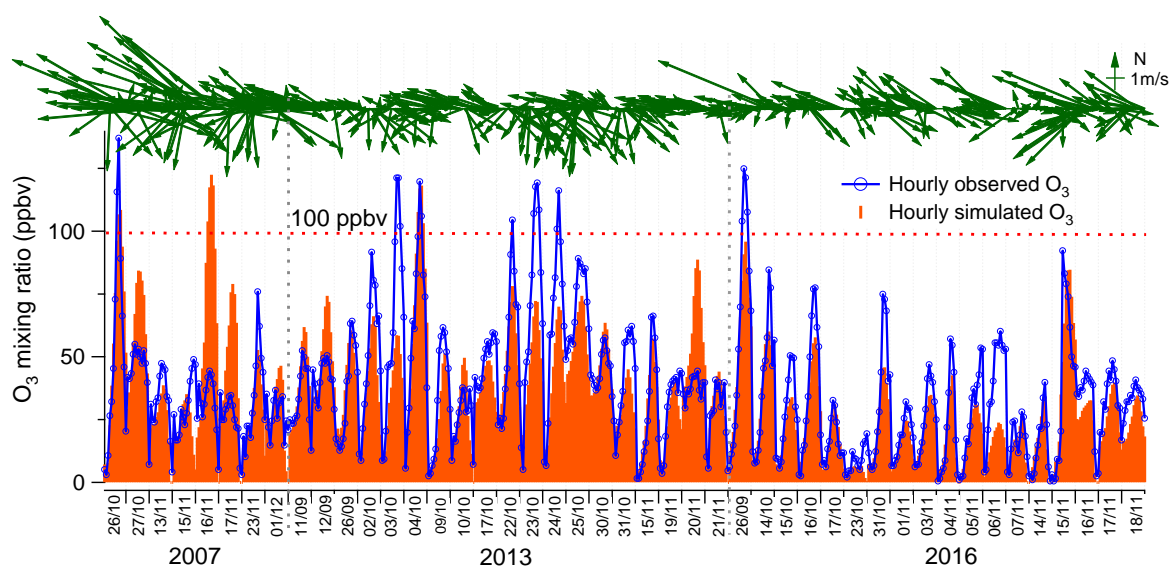
Figure 3. Hourly mixing ratio of the simulated and observed O_3 at TC during the VOC sampling periods in 2007, 2013 and 2016. The arrows represent the hourly wind sectors monitored at the sampling site.

3.2.2 Inter-annual variations of the locally produced and regional transported O_3

As discussed in section 2.5, the simulated O_3 in scenario A could be regarded as the locally produced O_3. Therefore, the differences between the observed O_3 and O_3 simulated in scenario A were treated as the regionally transported O_3 (Wang et al., 2017a). It is noteworthy that some negative values were generated with this method, corresponding to the dilution of the south winds to the locally produced O_3 as elaborated in section 3.2.1. Figure 4 shows the hourly mixing ratios of the observed, local and regional O_3 at TC in daytime hours (07:00-19:00 LT) of the three sampling campaigns. Overall, the observed O_3 was mainly (88.7±2.5%) contributed by the local photochemical production, with regional transport only accounting for 11.3±2.5% of the observed daily maximum O_3. However, regional transport was responsible for as high as 58.0±5.4% of the observed daily maximum O_3 in Hong Kong on the O_3 episode days when northerly winds prevailed, indicating the heavy O_3 burden superimposed by regional air masses from PRD. From 2007 to 2013, the simulated locally-produced O_3 remained statistically unchanged ($p>0.1$), in contrast to the increase of observed

443   O_3 and regional O_3 at rates of 1.78±0.05 ppbv yr^{-1} ($p<0.05$) and 1.77±0.04 ppbv yr^{-1} ($p<0.05$),

444   respectively, the same trends as those reported by Wang et al. (2017a) for the autumn O_3

445   during 2005-2013. However, the decease of the locally produced O_3 in the same period as

446   that simulated by Wang et al. (2017a) was not seen here according to the simulated O_3 in the

447   2007 and 2013 sampling campaigns. This discrepancy was likely caused by the limited

448   samples in this study, no OVOCs considered in Wang et al. (2017a) and/or the inexactly

449   same study periods between the two studies. Instead, we found that the locally produced O_3

450   showed a significant decline at a rate of -5.52±0.05 ppbv yr^{-1} during 2013-2016 ($p<0.05$),

451   when the regionally transported O_3 did not change ($p=0.32$), resulting in a downward trend (-

452   5.31±0.07) of the observed O_3. As such, the increase of the observed O_3 from 2007 to 2013

453   was reversed by the decrease between 2013 and 2016, leading to an overall decreasing trend

454   of the observed O_3 during 2007-2016 (rate = -0.57±0.03 ppbv yr^{-1}, $p<0.05$).

455
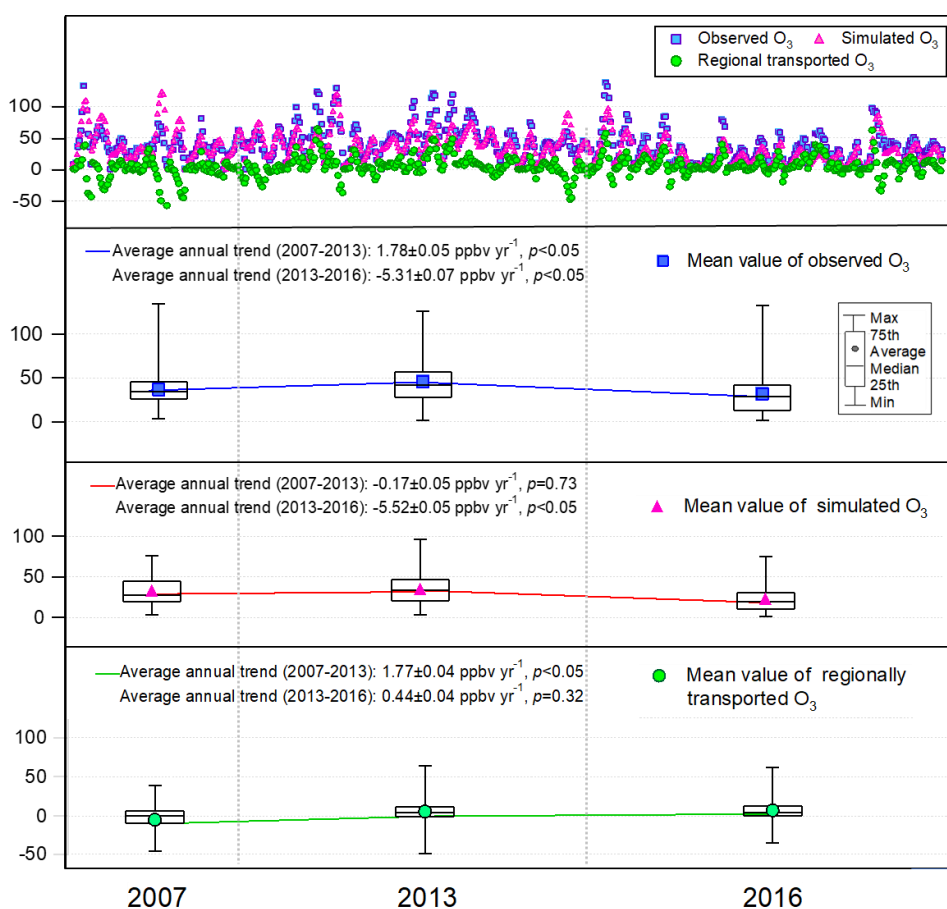
Figure 4. Hourly values (first panel) and the throughout-campaign statistical results (second to fourth panels) of the observed, simulated (locally-produced) and regional O_3 mixing ratios in daytime hours (07:00 – 19:00 LT) in the three sampling campaigns.

The significant alleviation of O_3 pollution in Hong Kong from 2013 to 2016 might be related to the measures taken to control the emissions of O_3 precursors in Hong Kong and in mainland China. The effectiveness of the actions launched by Hong Kong government in O_3 abatement was fully demonstrated in previous studies (Xue et al., 2014a; Lyu et al., 2017a; Wang et al., 2017a), and would be further evaluated in this study (section 3.4). Besides, the emission controls in mainland China might contribute to the decrease of O_3 or at least lessen the regional O_3 burden in this period. For example, the China's NO_x emissions for the first time showed a decreasing trend from 2013, benefited from the implementation of the China's Clean Air Action Plan (Zheng et al., 2018). Furthermore, we looked into the monthly average O_3 observed at the 12 air quality monitoring stations across the inland PRD, including three regional monitoring stations, *i.e.* Tianhu, Wanqingsha and Jinguowan, and nine urban monitoring stations, *i.e.* Xiapu, Jinjuzui, Donghu, Tangjia, Liyuan, Huijingcheng, Zimaling, Luhu and Chengzhong (https://www.epd.gov.hk/epd/sc_chi/resources_pub /publications/m_report.html). As shown in Figure 5, O_3 at these stations remained relatively stable (*p*=0.68) during 2006-2013, which however showed a contrastively decreasing trend at a rate of -1.27±0.25 ppbv yr^{-1} from 2013 to 2016. This corroborated our modelling results that the regional contribution to O_3 in Hong Kong ceased increasing or even began to decrease since 2013. While the substantial decrease of NO_x was a plausible reason for the alleviated regional O_3 pollution, meteorological variations might also play roles in modulating O_3 variations in these years (Li et al., 2019). However, analyses on the causes are out of the scope of this study. In addition to the reduced local formation and regional

480   transport of O_3, the more favourable meteorological conditions in 2016 might be another

481   reason of the O_3 decrease, as discussed in section 3.1.
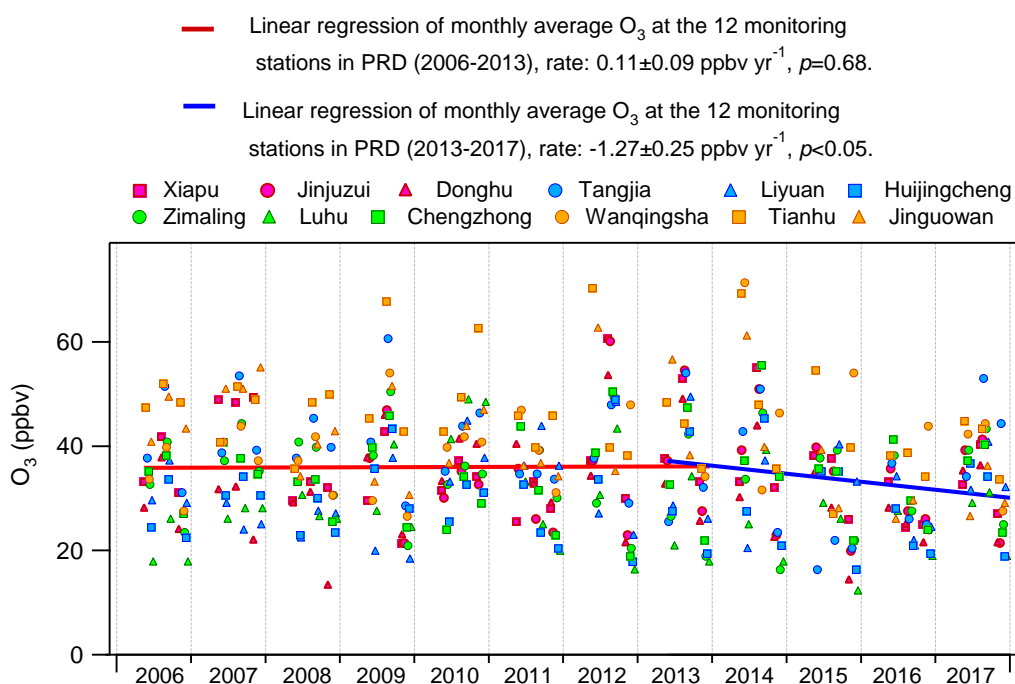
482

483   Figure 5. Trends of the observed monthly average O_3 at the 12 air quality monitoring stations

484   in inland PRD.

3.3 Local production and destruction pathways of O_3 and OH radical

3.3.1 In-situ net O_3 production

487   Figure 6 shows the average diurnal profiles of the simulated O_3 production and destruction

488   pathways during the three sampling campaigns. Also shown are the average diurnal cycles of

489   the simulated O_3. The shift of the peaks between the net O_3 production rate and the simulated

490   O_3 was due to the accumulation of the newly generated O_3 over time in the model, which was

491   also true in the real situations. The reactions between NO_2 and O_3, leading to the formation of

492   NO_3 and N_2O_5, in addition to dry deposition and aloft exchange, were the main depletions of

493   the simulated O_3 in the late afternoon. Consistent with previous studies (Kanaya et al., 2009;

494   Liu et al., 2012; Xue et al., 2014b), these pathways were not included in the calculation of the

495   net O_3 production rate, because we mainly focused on the photochemical processes in the

496   hours when O_3 was accumulated. It was found that the reaction between HO_2 with NO

497   dominated the O_3 production rates in all the cases, with an average rate of 3.7±0.7 ppbv h^{-1}

498   (56.5±1.1%, percentage of the total O_3 production rate, same below), 2.5±0.3 ppbv h^{-1}

499   (64.3±0.8%) and 1.4±0.2 ppbv h^{-1} (67.7±0.7%) in the 2007, 2013 and 2016 sampling

500   campaigns, respectively. In addition, the sum of the reaction rates between RO_2 radicals and

501   NO contributed 3.0±0.6 ppbv h^{-1} (43.5±1.1%), 1.5±0.2 ppbv h^{-1} (35.7±0.8%) and

502   0.7±0.1 ppbv h^{-1} (32.3±0.7%) to the O_3 production rate in 2007, 2013 and 2016, respectively.

503   The formation of HNO_3 though the reaction between OH and NO_2 served as the main

504   scavenger pathway of O_3, as NO_2 would be photolyzed and produce O_3 otherwise. On

505   average, O_3 was consumed in this way at a rate of -1.3±0.2 ppbv h^{-1} (80.7±3.3%, percentage

506   of the total O_3 destruction rate, same below), -1.0±0.1 ppbv h^{-1} (79.3±1.8%)

507   and -0.6±0.07 ppbv h^{-1} (81.6±2.0%) in 2007, 2013 and 2016, respectively. The photolysis of

508   O_3 was the second contributor to O_3 destruction, with an average contribution of -0.11±0.01

509   ppbv h^{-1} (8.5±0.5%) for the three sampling periods. Besides, the ozonolysis of unsaturated

510   VOCs and the reactions between O_3 and radicals (OH and HO_2) were responsible for 3.5±0.3%

511   and 1.7±0.2% of the total destruction rate of the locally produced O_3, respectively.

512   Overall, the net local O_3 production rate decreased from 5.2±1.1 ppbv h^{-1} in 2007, to

513   2.7±0.4 ppbv h^{-1} in 2013, till 1.4±0.3 ppbv h^{-1} in 2016, corresponding to the decline of the

514   locally produced O_3 through 2007 to 2016 (Section 3.2.2).
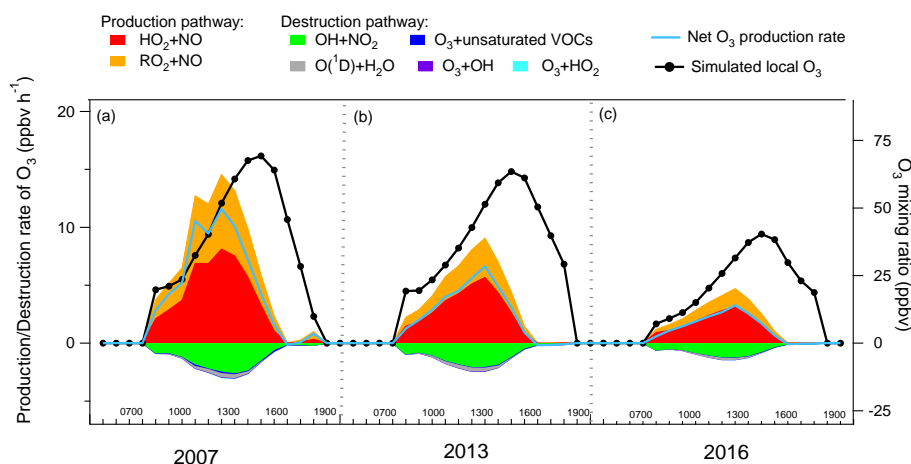
Figure 6. Average diurnal profiles of the local O_3 production and destruction rates in the sampling campaigns of (a) 2007, (b) 2013 and (c) 2016.

3.3.2 Recycling of OH radical

As one of the most important radicals in the atmosphere, OH initiates the oxidation of VOCs, leading to O_3 formation. Figure 7 presents the average diurnal profiles of the simulated OH and the formation and loss pathways dominating the recycling of OH during the three sampling periods, which roughly followed the typical pattern of the intensities of photochemical reactions, *i.e.* higher at noon and lower at the beginning and end of the day. On average, the simulated OH concentration was comparable (*p*=0.4) between the 2007 sampling campaign ($1.6\pm0.3\times10^6$ molecules cm^{-3}) and the 2013 sampling campaign ($1.5\pm0.2\times10^6$ molecules cm^{-3}), but it decreased (*p*<0.05) to $1.0\pm0.2\times10^6$ molecules cm^{-3} in the 2016 sampling campaign.

As expected, the formation and loss rates of OH were basically balanced in all the cases. OH was mainly formed from the reaction of HO_2+NO, which accounted for $69.8\pm1.1\%$ of the total OH production rate over the three sampling campaigns. The photolysis of HONO ranked the second in supplying OH with the contribution of $22.0\pm1.4\%$. As stated in section 2.4.2, the average diurnal cycle of HONO measured at TC in 2011 was adopted in the simulations. To assess the uncertainties, we also calculated the HONO concentrations according to the

534   measured HONO/NO$_x$ ratios and the NO$_x$ concentrations at TC in the three sampling

535   campaigns (Figure S5). The uncertainties in HONO concentrations and in the contributions of

536   HONO to OH formation and loss rates are discussed in Text S3. The formation of OH from

537   HONO photolysis was most efficient in the early morning, which was explained by the

538   morning peak of HONO concentration, due to the nocturnal heterogeneous formation and the

539   vehicle emissions in morning rush hours. Apart from the two dominant pathways, O$_3$

540   photolysis (6.3±0.2%), ozonolysis of unsaturated VOCs (1.5±0.2%) and H$_2$O$_2$ photolysis

541   (0.2±0.01%) also made some contributions to the formation of OH, with the highest rates at

542   noon or in the early afternoon when the productions of O$_3$ and H$_2$O$_2$ were the most intensive.

543   To sum up, the total formation rates of OH from the primary sources (photolysis of HONO,

544   O$_3$ and H$_2$O$_2$, and ozonolysis of VOCs) were lower than the recycling rates of OH (HO$_2$+NO)

545   throughout the day at TC, consistent with the results in Xue et al. (2016) simulated at the

546   same site. The dominant role of HO$_2$+NO in OH formation at TC (average contribution of

547   69.8±1.1%) might be related to the abundant NO at this site. The same pathway was

548   simulated and accounted for only 42.7±0.2% of the total OH formation rate at an island more

549   than 40 km away from Hong Kong with very low NO concentrations, *i.e.* maximum of 0.56

550   ppbv (Wang et al., 2018a).

551   OH was mainly depleted by the reactions with VOCs (32.3±1.2%), NO$_2$ (31.9±0.9%), CO

552   (19.3±0.6%) and NO (16.5±1.1%). The reaction rates of OH+NO (formation rates of HONO)

553   had the highest values in the morning, approximately in line with the diurnal pattern of the

554   HONO photolysis rates, which however were not completely balanced due to the constraint

555   of HONO to observations in the model. The average net photolysis rates of HONO

556   (differences between the HONO photolysis and formation rates) were $0.68\pm0.21\times10^6$,

557    $0.70\pm0.12\times10^6$ and $0.87\pm0.12\times10^6$ molecules cm^{-3} s^{-1} in the 2007, 2013 and 2016 sampling

558   campaigns, respectively. The losses of OH through the other pathways all exhibited the

559   highest efficiencies at noon or in the early afternoon. It should be noted that the reaction

560   between OH and NO_2 was not only the sink of OH but also a termination reaction in the

561   photochemical system. In comparison, the termination reaction rates were lower than the OH

562   formation rates from the primary sources (photolysis of HONO, O_3 and H_2O_2, and ozonolysis

563   of VOCs) in the morning (7:00 – 10:00 LT), which were reversed in the following hours of

564   the day due to the increases in OH concentrations.

565   Consistent with the variations of the local O_3 production, both the local formation and loss

566   rates of OH decreased through 2007 to 2016 ($p<0.05$), with much more obvious reductions in

567   the later phase (2013-2016). On one hand, the continuous reduction of VOCs resulted in

568   lower HO_2 and RO_2 concentrations (Figure S6), hence the lower production rate of OH

569   through the reaction of HO_2+NO. At the same time, the destruction rates of OH also

570   decreased due to the reductions of OH and the O_3 precursors, except for CO (Figure 7 and

571   Table 1). The decreases of the OH production and destruction rates indicated that the

572   propagation of the reaction cycles, namely the recycling of OH, became slower from 2007 to

573   2016. This also explained why the locally produced O_3 decreased in these ten years, since O_3

574   is formed with the consumption and recycling of OH radical.
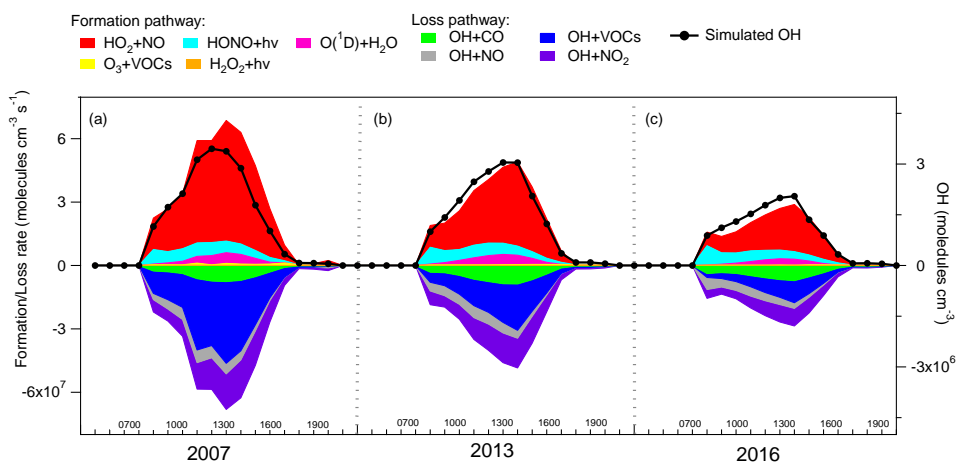
576   Figure 7. Average diurnal cycles of the OH formation and loss rates during the sampling

577 periods in (a) 2007, (b) 2013 and (c) 2016.

3.4 Source contributions to the production of O_3 and radicals

3.4.1 Source apportionment

To resolve the sources of O_3 precursors, 27 species, including CO, NO, NO_2, 12 alkanes, 4 alkenes and 8 aromatics, were applied to PMF for source apportionment. These species were either of high abundances or typical tracers of VOC sources in Hong Kong. Source apportionment was conducted for a total of 414 samples covering the three sampling periods, so that the uncertainty of the source apportionment results could be reduced, compared to separate source apportionments for each of the three sampling periods. Figure 8 shows the average profiles of the six sources resolved by PMF. The modelling errors were estimated with the bootstrap method integrated in PMF (Brown et al., 2015).

Factor 1 was assigned as the combination of LPG usage and gasoline evaporation, in view of the high loadings of C_2-C_5 hydrocarbons. Specifically, propane and *i*-/*n*-butanes are the main components of LPG in Hong Kong, and gasoline evaporation generally contains large quantities of *i*-/*n*-pentanes, in particularly *i*-pentane (Guo et al., 2013a; Lyu et al., 2017a). Factor 2 was characterized by moderate to high percentages of *i*-/*n*-pentanes and TEX (toluene, ethylbenzene and xylenes). These species are commonly seen in gasoline exhausts. Therefore, we defined this factor as gasoline exhausts. Both the third and fourth factors indicated solvent-related emissions. While Factor 3 likely represented household solvent usage, due to the dominance of hexane and hexane isomer (3-methylpentane) (Ling and Guo, 2014; Ou et al., 2015), Factor 4 was more related to emissions from coatings and paints, in view of the dominance of the aromatics (Ling and Guo, 2014). Factor 5 was distinguished by the high concentrations of ethane, ethene, ethyne and benzene, together with the relatively heavy (C_7-C_{10}) alkanes, which are typical species in diesel exhausts (Schauer et al., 1999; Kashdan et al., 2008; Sahoo et al., 2011). Therefore, this factor was designated as diesel

27

602   exhausts. The last factor denoted for biogenic emissions (BVOCs), due to the exclusive

603   dominance of isoprene (Guenther, 2006).
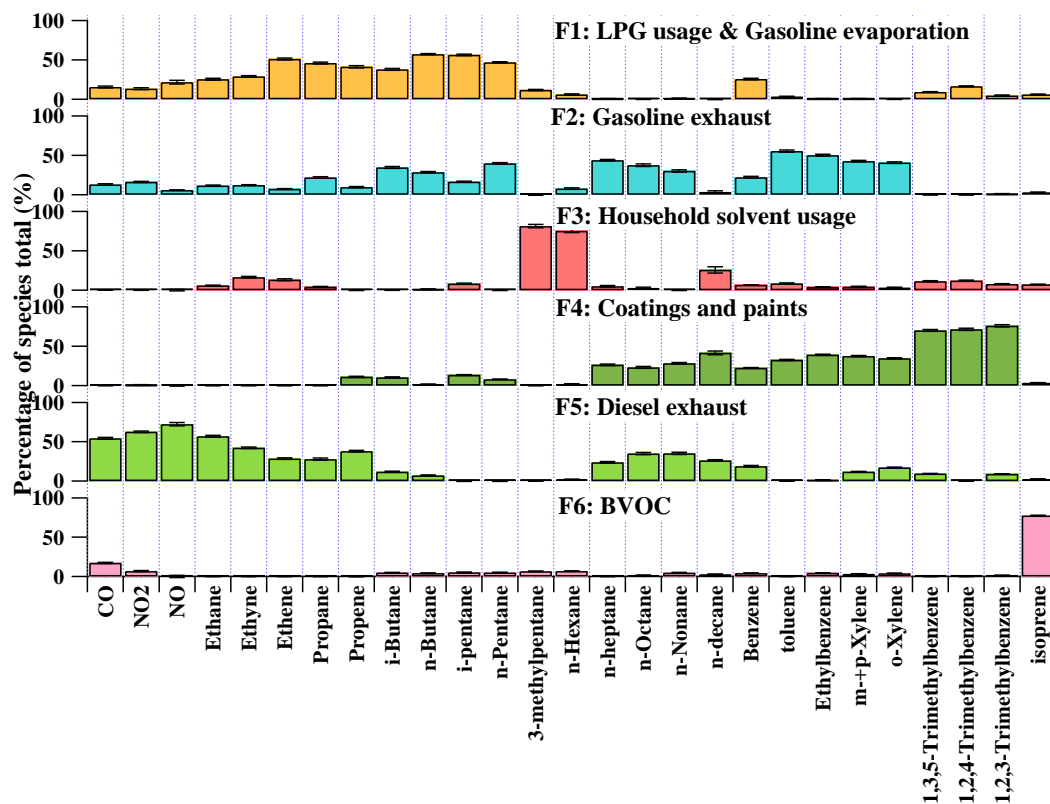
604

605   Figure 8. Average profiles of the O_3 precursors sources at TC in the three sampling

606   campaigns. The uncertainties were estimated with the bootstrap method in PMF.

607   Figure S7 presents the total mixing ratio of VOCs emitted from each individual source

608   extracted from PMF during the three sampling periods in Hong Kong. The VOC emissions

609   from LPG usage and gasoline evaporation decreased significantly ($p<0.05$) at a rate of -

610   2.61±0.03 ppbv yr^{-1} from 2007 to 2016. However, the VOCs in association with gasoline

611   exhausts experienced an increase (rate = 1.32±0.02 ppbv yr^{-1}, $p<0.05$) in these years,

612   indicating that the reduction of VOC emissions from LPG usage and gasoline evaporation

613   was not attributable to the change in emissions of gasoline-fuelled vehicles. Insight into the

614   mixing ratios of propane and i-/n-butanes (LPG tracers) in this source revealed a significant

615   decline from 3.51±0.52 ppbv in the 2007 sampling campaign to 1.27±0.11 ppbv in the 2016

28

616   sampling campaign. Therefore, the reduction of VOC emissions from LPG usage was most

617   likely the reason of the decrease of VOCs allocated to the source of LPG usage and gasoline

618   evaporation. In fact, it was confirmed by our previous studies (Lyu et al., 2016b; Yao et al.,

619   2019) that the replacement of catalytic converters on LPG-fuelled vehicles during September

620   2013-May 2014 effectively reduced the VOC emissions from LPG-fuelled vehicles in Hong

621   Kong. In addition, the variations in LPG usage in inland PRD, where LPG was extensively

622   used as vehicular and domestic fuels (Liu et al., 2008), might also contribute to the emission

623   reduction of VOCs, in view of the decrease of LPG tracers in this source from 2007

624   (3.51±0.52 ppbv) to 2013 (2.04±0.27 ppbv), when no control was performed against LPG

625   fuelled vehicle emissions in Hong Kong. The VOCs emitted from solvent usage (including

626   the household solvent, coatings and paints) also decreased significantly ($p<0.05$) from 2007

627   to 2016, likely benefiting from the actions taken to restrict the VOC contents in solvent

628   products starting from 2007 (phase I) and 2010 (phase II) in Hong Kong (Lyu et al., 2017a).

629   VOCs attributable to diesel exhausts decreased ($p<0.05$) from the 2007 (2.6±0.3 ppbv) to

630   2013 sampling campaign (2.0±0.2 ppbv), which however were unchanged between 2013 and

631   2016 (2.2±0.2 ppbv). In fact, a subsidy program has been implemented in Hong Kong since

632   2007 to progressively eliminate the pre-Euro IV diesel vehicles or to upgrade their emission

633   standards to Euro IV (HKEPD, 2017b), and the effectiveness of this program in VOC

634   reductions till 2013 was confirmed by Lyu et al. (2017a) with the online measurement data at

635   the same site. However, while the phase III of this program (2014-2019) is still ongoing, the

636   VOCs emitted from diesel vehicles remained stable between the 2013 and 2016 sampling

637   campaigns. This undesirable result might be due to the fact that the actions were mainly

638   targeted at the pre-Euro, Euro I and Euro II diesel vehicles before 2013, whereas the phase III

639   of the program initiated in 2014 focused on the Euro III vehicles (HKEPD, 2017b, 2018).

640   Since the former were vehicles with higher emissions, it is not unreasonable that reduction of

641   VOCs was more discernible between 2007 and 2013. Further, the effectiveness of the phase

642   III program might be somewhat offset by the wearing-out of the pre-existing vehicles and the

643   increase of diesel vehicle populations (Competition Commission, 2017). Further evaluation

644   with more data in a longer period is recommended. At last, the increase of BVOCs from 2007

645   to 2013 but comparable levels between 2013 and 2016 seemed to be related to the lower

646   ($p<0.05$) temperature in the 2007 sampling campaign (Figure S8 and Table S6). Besides, the

647   more frequent (62.8%) southeast winds from SCS with higher wind speeds (2.3 ± 0.2 m s^{-1})

648   might dilute BVOCs emitted from the terrestrial plants in the 2007 sampling campaign.

649   **3.4.2 Source contributions to O$_3$ production**

650   Figure 9 presents the contributions of VOCs emitted from individual sources to the

651   production and destruction rates of O$_3$, as well as the simulated contributions to the O$_3$

652   mixing ratios. NO$_x$ was not included in these analyses, because of its relatively high

653   uncertainties in source apportionment results due to the short lifetimes. Consistent with the

654   O$_3$ production and destruction in the whole air, the pathway of HO$_2$+NO dominated over the

655   reactions between RO$_2$ and NO in O$_3$ production for all the individual sources. The

656   destruction of O$_3$ was mainly driven by NO$_2$ reacting with OH. For the net O$_3$ production rate,

657   VOCs attributable to the coatings and paints made the largest contribution (0.38 ± 0.05 ppbv h^{-1}

658   ), followed by gasoline exhausts (0.22 ± 0.03ppbv h^{-1}), LPG and gasoline evaporation

659   (0.21 ± 0.03ppbv h^{-1}), BVOCs (0.19 ± 0.03ppbv h^{-1}), household solvent usage (0.15 ± 0.04 ppbv

660   h^{-1}) and diesel exhausts (0.13 ± 0.01ppbv h^{-1}). Despite some peak shifts for the reasons

661   illustrated in section 3.3.1, the O$_3$ mixing ratios elevated by the individual sources followed

662   the same pattern as the net O$_3$ production rates, with the highest O$_3$ enhancement (1.92 ± 0.21

663   ppbv) by the source of coatings and paints and the lowest increase by household solvent

664   usage (0.86 ± 0.06 ppbv) and diesel exhausts (0.83 ± 0.06 ppbv). The contributions of source-

665   specific VOCs to O$_3$ production, particularly the importance of solvent usage in O$_3$ formation

666   in Hong Kong, were generally in line with previous studies (Ling and Guo, 2014; Ou et al.,

667   2015). This was actually expected according to the reactivity of major VOCs in each source.

668   For example, the TEX in the source of coatings and paints (Figure 8) have been identified to

669   be of high O_3 formation potentials (Lau et al., 2010; Ling et al., 2011, 2013). However, the

670   PBM-MCM model simulations enabled us to quantitatively evaluate the contributions of

671   VOC sources to O_3 production rates.
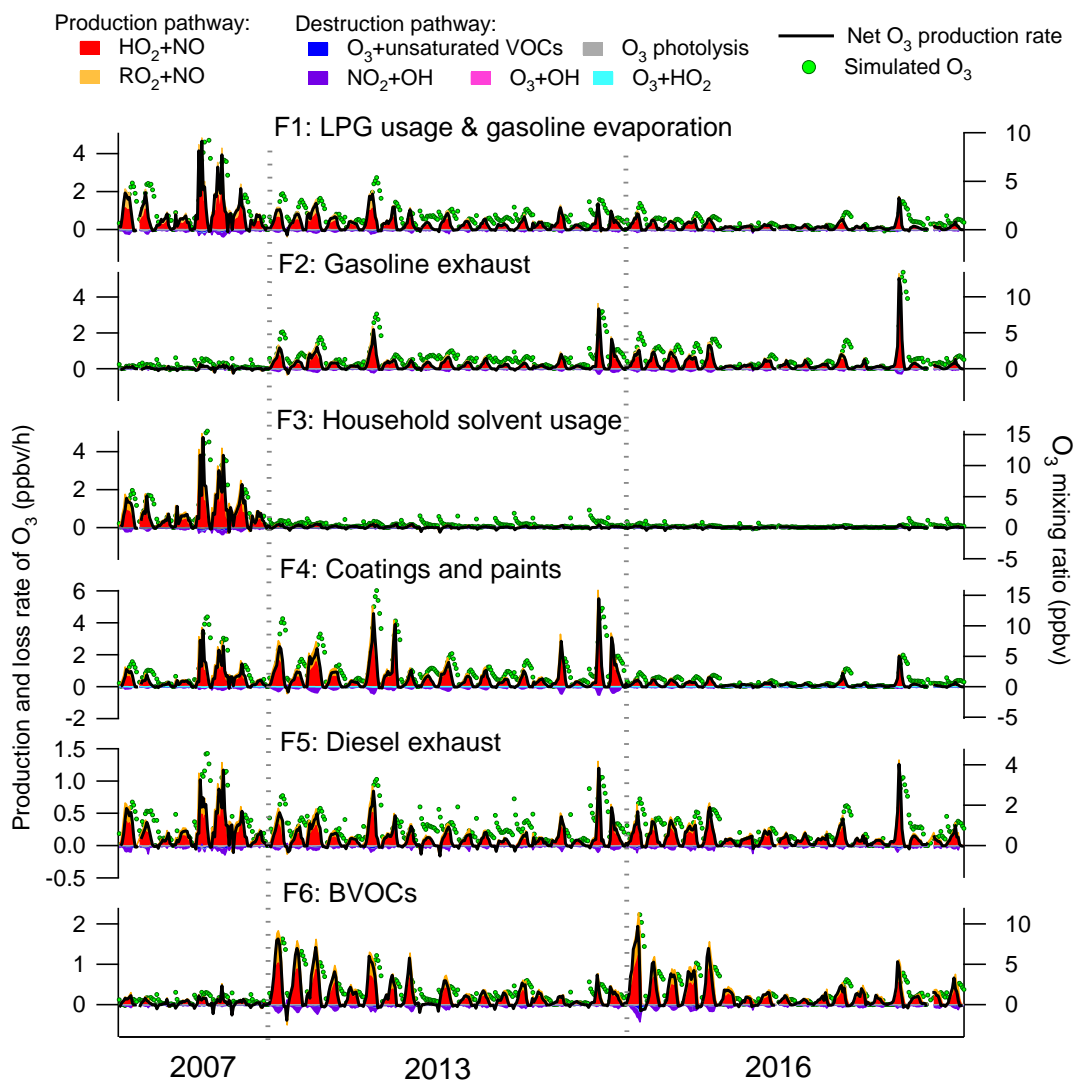
672

673   Figure 9. Contributions of VOCs in individual sources to the production and destruction rates

674   of O_3 and to the O_3 mixing ratios in the three sampling campaigns.

675 From a historical perspective, we found that the contribution of LPG usage and gasoline

676 evaporation to O_3 production significantly decreased ($p<0.05$) from 2007 to 2016 sampling

677 campaign (2007: 0.51 ± 0.11 ppbv h^{-1}; 2013: 0.20 ± 0.03 ppbv h^{-1}; 2016: 0.10 ± 0.02 ppbv h^{-1}),

678 which coincided with the variations of VOCs emitted from LPG-fuelled vehicles as discussed

679 above. Gasoline exhaust contributed much less ($p<0.05$) to the net O_3 production rate in 2007

680 (0.02 ± 0.01ppbv h^{-1}), than those in 2013 (0.26 ± 0.05ppbv h^{-1}) and 2016 (0.27 ± 0.07ppbv h^{-1}),

681 in line with the variations of VOCs emitted from this source. The reductions of VOC

682 emissions from solvents also resulted in the consistent decrease of the net O_3 production rate

683 from 1.22 ± 0.17 ppbv h^{-1} in the 2007 to 0.14 ± 0.05 ppbv h^{-1} in the 2016 sampling campaign.

684 The O_3 production rates contributed by VOCs in diesel exhausts were reduced from 2007

685 (0.21 ± 0.05 ppbv h^{-1}) to 2013 (0.11 ± 0.02 ppbv h^{-1}) and remained unchanged thereafter (2016:

686 0.11 ± 0.02 ppbv/h). The O_3 production rate traceable to BVOCs showed a significant increase

687 from 2007 (0.04 ± 0.02 ppbv h^{-1}) to 2016 (0.22 ± 0.04 ppbv h^{-1}), since the mixing ratios of

688 BVOCs significantly increased ($p<0.05$) in these years. It is noteworthy that the changes in

689 meteorological conditions in these three sampling campaigns might also partially account for

690 the variations in the source contributions to O_3 production. For example, the 2013 sampling

691 campaign was characterized by the relatively higher temperature and lowest relative humidity

692 among the three sampling periods, which favoured O_3 formation in 2013 (Table S6). Besides,

693 due to limited samples in this study, we recommend further assessments with more data in

694 longer periods to be carried out in future study.

695 **4 Conclusions**

696 Photochemical pollution with high and increasing concentrations of O_3 has been an important

697 environmental issue in South China. With the observation data of O_3 and its precursors at a

698 suburban site in Hong Kong, downwind of South China, this study analysed the inter-annual

699 variations of O_3 and its photochemistry, as well as the contributions of VOC sources to the

700 local O_3 production rates in 2007, 2013 and 2016. To our knowledge, this is the first time that

701 a substantial alleviation of O_3 pollution in this region was identified between 2013 and 2016,

702 in contrast to the repeatedly confirmed O_3 increase before 2013. In addition to the changes in

703 meteorological conditions among the three sampling campaigns, the termination of the rise in

704 regionally transported O_3 and the decrease of the local O_3 production rate contributed to the

705 decline of O_3 in the later period. The emission reductions (particularly for NO_x) in mainland

706 China starting from 2013, the year when the China's Clean Air Action Plan was launched,

707 might more or less play a role in ceasing the increase of regional O_3. In Hong Kong, the

708 replacement of catalytic converters and the constraints of VOC contents in solvent products

709 led to the reductions of VOC emissions from LPG-fuelled vehicles and solvent usage,

710 respectively. As a result, the local O_3 production rate and the recycling rate of OH radical

711 decreased substantially from 2013 to 2016. Though the variations in meteorological

712 conditions and the limited sample size might somewhat introduce uncertainties to the

713 conclusions drawn from the present study, it is plausible that the local and regional

714 interventions were effective on the control of O_3 pollution in Hong Kong. Nevertheless,

715 studies with more data in longer periods should be conducted, not only in Hong Kong but

716 also in mainland China where O_3 is still increasing in most of the territories.

717 **Author contribution**

718 Hai Guo and Fei Jiang initiated and designed the experiments, and Xufei Liu and Xiaopu Lyu

719 carried them out. Xiaopu Lyu and Yu Wang developed the model code and performed the

720 simulations. Xufei Liu and Xiaopu Lyu prepared the manuscript and Hai Guo finalized the

721 manuscript with contributions from all co-authors.

722 **Acknowledgements**

730 **References**

731 Ashmore, M. R.: Assessing the future global impacts of ozone on vegetation, Plant. Cell.

732 Environ., 28, 949-964, 2005.

733 Bell, M. L., McDermott, A., Zeger, S. L., Samet, J. M., and Dominici, F.: Ozone and short-

734 term mortality in 95 US urban communities, 1987-2000, JAMA, 292, 2372-2378, 2004.

735 Brown, S. G., Frankel, A., and Hafner, H. R.: Source apportionment of VOCs in the Los

736 Angeles area using positive matrix factorization, Atmos. Environ., 41, 227-237, 2007.

737 Brown, S. G., Eberly, S., Paatero, P., and Norris, G. A.: Methods for estimating uncertainty in

738 PMF solutions, Sci. Total Environ., 518, 626-635, 2015.

739 Census and Statistics Department (CSD), 2011 Population Census in Hong Kong, available at:

740 https://www.census2011.gov.hk/en/constituency-area-i.html (last access: 25 October 2018),

741 2011.

742 Census and Statistics Department (CSD), District profile for 2016 Population Census in Hong

743 Kong, available at: https://www.bycensus2016.gov.hk/en/bc-dp.html (last access: 25 October

744 2018), 2018.

745 Cheng, H. R., Guo, H., Wang, X. M., Saunders, S. M., Lam, S. H. M., Jiang, F., Wang, T. J.,

746 Ding, A. J., Lee, S. C., and Ho, K. F.: On the relationship between ozone and its precursors in

the Pearl River Delta: application of an observation-based model (OBM), Environ. Sci. Pollut. Res., 17, 547-560, 2010.

Cheng, H. R., Saunders, S. M., Guo, H., Louie, P. K. K., and Jiang, F.: Photochemical trajectory modeling of ozone concentrations in Hong Kong, Environ. Pollut, 180, 101-110, 2013.

Cheng, Y., Lee, S. C., Huang, Y., Ho, K. F., Ho, S. S. H., Yau, P. S., Louie, P. K. K., and Zhang, R. J.: Diurnal and seasonal trends of carbonyl compounds in roadside, urban, and suburban environment of Hong Kong, Atmos. Environ., 89, 43-51, 2014.

Chou, C. C. K, Liu, S. C., Lin, C. Y., Shiu, C. J., and Chang, K. H.: The trend of surface ozone in Taipei, Taiwan, and its causes: Implications for ozone control strategies, Atmos. Environ., 40, 3898-3908, 2006.

Colman, J. J., Swanson, A. L., Meinardi, S., Sive, B. C., Blake, D. R., and Rowland, F. S.: Description of the analysis of a wide range of volatile organic compounds in whole air samples collected during PEM-Tropics A and B, Anal. Chem., 73, 3723-3731, 2001.

Competition Commission: Report on Study into Hong Kong's Auto-fuel Market, available at: https://www.compcomm.hk/en/media/press/files/Full_Report_Auto_fuel_Market_Study_Rep ort_Eng.pdf (last access: 25 October 2018), 2017.

Cui, J., Pandey Deolal, S., Sprenger, M., Henne, S., Staehelin, J., Steinbacher, M., and Nédélec, P.: Free tropospheric ozone changes over Europe as observed at Jungfraujoch (1990–2008): An analysis based on backward trajectories, J. Geophys. Res. Atmos., 116, D10304, https://doi.org/10.1029/2010JD015154, 2011.

Cui, L., Zhang, Z., Huang, Y., Lee, S. C., Blake, D. R., Ho, K. F., Wang, B., Gao, Y., Wang, X. M., and Louie, P. K. K. Measuring OVOCs and VOCs by PTR-MS in an urban roadside microenvironment of Hong Kong: relative humidity and temperature dependence, and field inter-comparisons, Atmos. Meas. Tech., 9, 5763-5779, 2016.

772   Derwent, R. G., Manning, A. J., Simmonds, P. G., Spain, T. G., and O'Doherty, S.: Analysis

773   and interpretation of 25 years of ozone observations at the Mace Head Atmospheric Research

774   Station on the Atlantic Ocean coast of Ireland from 1987 to 2012, Atmos. Environ., 80, 361-

775   368, 2013.

776   Ding, A. J., Wang, T., Zhao, M., Wang, T. J., and Li, Z. K.: Simulation of sea-land breezes

777   and a discussion of their implications on the transport of air pollution during a multi-day

778   ozone episode in the Pearl River Delta of China, Atmos. Environ., 38, 6737-6750, 2004.

779   Ding, A.J., Wang, T., Thouret, V., Cammas, J., and Nédélec, P.: Tropospheric ozone

780   climatology over Beijing: analysis of aircraft data from the MOZAIC program, Atmos. Chem.

781   Phys., 8, 1-13, 2008.

782   Dongguan Environment Protection Department (DGEPD), Clean air action plan in Pearl

783   River Delta region, Phase II (2013-2015), available at: http://dgepb.dg.gov.cn

784   /publicfiles///business/htmlfiles/dgepb/cmsmedia/document/doc172679.pdf   (last access: 25

785   October 2018), 2013.

786   Guenther, A., Karl, T., Harley, P., Wiedinmyer, C., Palmer, P.I., and Geron, C.: Estimates of

787   global terrestrial isoprene emissions using MEGAN (Model of Emissions of Gases and

788   Aerosols from Nature), Atmos. Chem. Phys., 6, 3181-3210, 2006.

789   George, I. J., Matthews, P. S. J., Whalley, L. K., Brooks, B., Goddard, A., Baeza-Romero, M.

790   T., and Heard, D. E.: Measurements of uptake coefficients for heterogeneous loss of HO_2

791   onto submicron inorganic salt aerosols, Phys. Chem. Chem. Phys., 15, 12829-12845, 2013.

792   Guo, H., Jiang, F., Cheng, H. R., Simpson, I. J., Wang, X. M., Ding, A. J., Wang, T. J.,

793   Saunders, S. M., Wang, T., Lam, S. H. M., Blake, D. R., Zhang, Y. L., and Xie, M.:

794   Concurrent observations of air pollutants at two sites in the Pearl River Delta and the

795   implication of regional transport, Atmos. Chem. Phys., 9, 7343-7360, 2009.

796 Guo, H., Cheng, H. R., Ling, Z. H., Louie, P. K. K., and Ayoko, G. A.: Which emission

797 sources are responsible for the volatile organic compounds in the atmosphere of Pearl River

798 Delta? J. Hazard. Mater., 188, 116-124, 2011.

799 Guo, H., Ling, Z. H., Cheung, K., Jiang, F., Wang, D. W., Simpson, I. J., Barletta, B.,

800 Meinardi, S., Wang, T. J., Wang, X. M., Saunders, S. M., and Blake, D. R.: Characterization

801 of photochemical pollution at different elevations in mountainous areas in Hong Kong,

802 Atmos. Chem. Phys., 13, 3881-3898, 2013a.

803 Guo, H., Ling, Z. H., Cheung, K., Wang, D. W., Simpson, I. J., and Blake, D. R.: Acetone in

804 the atmosphere of Hong Kong: Abundance, sources and photochemical precursors, Atmos.

805 Environ., 65, 80-88, 2013b.

806 Guo, H., Ling, Z. H., Cheng, H. R., Simpson, I. J., Lyu, X. P., Wang, X. M., Shao, M., Lu, H.

807 X., Ayoko, G., Zhang, Y. L. and Saunders, S. M.: Tropospheric volatile organic compounds

808 in China, Sci. Total Environ., 574, 1021-1043, 2017.

809 Hong Kong Environmental Protection Department (HKEPD): Inquire and Download Air

810 Quality Monitoring Data, available at: epic.epd.gov.hk/ca/uid/airdata (last access: 25 October

811 2018), 2017a.

812 Hong Kong Environmental Protection Department (HKEPD): Cleaning the Air at Street

813 Level, available at: http://www.epd.gov.hk/epd/english/environmentinhk/air/prob_solutions

814 /strategies_apc.html (last access: 25 October 2018), 2017b.

815 Hong Kong Environmental Protection Department (HKEPD): Phasing Out Pre-Euro IV

816 Diesel Commercial Vehicles, available at: https://www.epd.gov.hk/epd/english

817 /environmentinhk/air/prob_solutions/Phasing_out_diesel_comm_veh.html (last access: 25

818 October 2018), 2018.

Hong Kong Observatory (HKO): Real-time Data Display from ENVF Atmospheric & Environmental Database, available at: http://envf.ust.hk/dataview/hko_wc/current/ (last access: 25 October 2018), 2017.

Huang, J. P., Fung, J. C., Lau, A. K., and Qin, Y.: Numerical simulation and process analysis of typhoon-related ozone episodes in Hong Kong, J. Geophys. Res. Atmos., 110, D05301, https://doi.org/10.1029/2004jd004914, 2005.

Jacob, D. J.: Introduction to atmospheric chemistry, Princeton University Press, Princeton, New Jersey, 1999.

Jenkin, M. E., Saunders, S. M., and Pilling, M. J.: The tropospheric degradation of volatile organic compounds: a protocol for mechanism development, Atmos. Environ., 31, 81-104, 1997.

Jenkin, M. E., Saunders, S. M., Wagner, V., and Pilling, M. J.: Protocol for the development of the Master Chemical Mechanism, MCM v3 (Part B): tropospheric degradation of aromatic volatile organic compounds, Atmos. Chem. Phys., 3, 181-193, 2003.

Jiang, F., Guo, H., Wang, T. J., Cheng, H. R., Wang, X. M., Simpson, I. J., Ding, A. J., Saunders, S. M., Lam, S. H. M., and Blake, D. R.: An ozone episode in the Pearl River Delta: Field observation and model simulation, J. Geophys. Res., 115, D22305, https://doi.org/10.1029/2009JD013583, 2010.

Jiang, Y. C., Zhao, T. L., Liu, J., Xu, X. D., Tan, C. H., Cheng, X. H., Bi, X. Y., Gan, J. B., You, J. F., and Zhao, S. Z.: Why does surface ozone peak before a typhoon landing in southeast China? Atmos. Chem. Phys., 15, 13331-13338, 2015.

Johnson, B.T.: Diesel engine emissions and their control, Platin. Met. Rev., 52, 23-37, 2008.

Kanaya, Y., Pochanart, P., Liu, Y., Li, J., Tanimoto, H., Kato, S., Suthawaree, J., Inomata, S., Taketani, F., Okuzawa, K., and Kawamura, K.: Rates and regimes of photochemical ozone

843 production over Central East China in June 2006: a box model analysis using comprehensive

844 measurements of ozone precursors, Atmos. Chem. Phys., 9, 7711-7723, 2009.

845 Kashdan, J.T.: Tracer LIF Visualisation Studies of Piston-Top Fuel Films in a Wall-Guided,

846 Low-NO$_x$ Diesel Engine, SAE Tech. Paper, 2008-01-2474, 2008.

847 Lakey, P. S. J., George, I. J., Whalley, L. K., Baeza-Romero, M. T., and Heard, D. E.:

848 Measurements of the HO$_2$ uptake coefficients onto single component organic aerosols,

849 Environ. Sci. Technol., 49, 4878-4885, 2015.

850 Lam, K. S., Wang, T. J., Wu, C. L., and Li, Y. S.: Study on an ozone episode in hot season in

851 Hong Kong and transboundary air pollution over Pearl River Delta region of China, Atmos.

852 Environ., 39, 1967-1977, 2005.

853 Lam, S. H. M., Saunders, S. M., Guo, H., Ling, Z. H., Jiang, F., Wang, X. M., and Wang, T.

854 J.: Modelling VOC source impacts on high ozone episode days observed at a mountain

855 summit in Hong Kong under the influence of mountain-valley breezes, Atmos. Environ., 81,

856 166-176, 2013.

857 Lau, A. K. H., Yuan, Z., Yu, J. Z., and Louie, P. K.: Source apportionment of ambient

858 volatile organic compounds in Hong Kong, Sci. Total Environ., 408, 4138-4149, 2010.

859 Lee, E., Chan, C. K., and Paatero, P.: Application of positive matrix factorization in source

860 apportionment of particulate pollutants in Hong Kong, Atmos. Environ., 33, 3201-3212, 1999.

861 Lefohn, A. S., Shadwick, D. and Oltmans, S. J.: Characterizing changes in surface ozone

862 levels in metropolitan and rural areas in the United States for 1980–2008 and 1994–2008,

863 Atmos. Environ., 44, 5199-5210, 2010.

864 Li, K., Jacob, D. J., Liao, H., Shen, L., Zhang, Q., and Bates, K. H.: Anthropogenic drivers of

865 2013–2017 trends in summer surface ozone in China, Proc. Natl. Acad. Sci. U. S. A., 116, 2,

866 422-427, 2019.

867   Lin, M., Horowitz, L.W., Payton, R., Fiore, A. M., and Tonnesen, G.: US surface ozone

868   trends and extremes from 1980 to 2014: quantifying the roles of rising Asian emissions,

869   domestic controls, wildfires, and climate, Atmos. Chem. Phys., 17, 2943-2970, 2017.

870   Ling, Z. H. and Guo, H.: Contribution of VOC sources to photochemical ozone formation

871   and its control policy implication in Hong Kong, Environ. Sci. Policy, 38, 180-191, 2014.

872   Ling, Z. H., Guo, H., Cheng, H. R., and Yu, Y. F.: Sources of ambient volatile organic

873   compounds and their contributions to photochemical ozone formation at a site in the Pearl

874   River Delta, southern China, Environ. Pollut., 159, 2310-2319, 2011.

875   Ling, Z. H., Guo, H., Zheng, J. Y., Louie, P. K. K., Cheng, H. R., Jiang, F., Cheung, K.,

876   Wong, L. C., and Feng, X. Q.: Establishing a conceptual model for photochemical ozone

877   pollution in subtropical Hong Kong, Atmos. Environ., 76, 208–220, 2013.

878   Ling, Z. H., Guo, H., Lam, S. H. M., Saunders, S. M., and Wang, T.: Atmospheric

879   photochemical reactivity and ozone production at two sites in Hong Kong: Application of a

880   Master Chemical Mechanism-photochemical box model, J. Geophys. Res. Atmos., 119,

881   10567-10582, 2014.

882   Ling, Z., Guo, H., Simpson, I. J., Saunders, S. M., Lam, S. H. M., Lyu, X., and Blake, D. R.:

883   New insight into the spatiotemporal variability and source apportionments of C_1–C_4 alkyl

884   nitrates in Hong Kong, Atmos. Chem. Phys., 16, 8141-8156, 2016a.

885   Ling, Z., Guo, H., Chen, G., Lam, S. H. M., and Fan, S.: Formaldehyde and acetaldehyde at

886   different elevations in mountainous areas in Hong Kong, Aerosol Air Qual. Res., 16, 1868-

887   1878, 2016b.

888   Liu, Y., Shao, M., Lu, S. H., Chang, C. C., Wang, J. L., and Chen, G.: Volatile Organic

889   Compound (VOC) measurements in the Pearl River Delta (PRD) region, China, Atmos.

890   Chem. Phys., 8, 1531-1545, 2008.

891   Liu, Z., Wang, Y., Gu, D., Zhao, C., Huey, L. G., Stickel, R., Liao, J., Shao, M., Zhu, T.,

892   Zeng, L., and Amoroso, A.: Summertime photochemistry during CAREBeijing-2007: RO_x

893   budgets and O_3 formation, Atmos. Chem. Phys., 12, 7737-7752, 2012.

894   Lyu, X. P., Ling, Z. H., Guo, H., Saunders, S. M., Lam, S. H. M., Wang, N., Wang, Y., Liu,

895   M., and Wang, T.: Re-examination of C_1-C_5 alkyl nitrates in Hong Kong using an

896   observation-based model, Atmos. Environ., 120, 28-37, 2015.

897   Lyu, X. P., Liu, M., Guo, H., Ling, Z. H., Wang, Y., Louie, P. K. K., and Luk, C. W. Y.:

898   Spatiotemporal variation of ozone precursors and ozone formation in Hong Kong: grid field

899   measurement and modelling study, Sci. Total Environ., 569, 1341-1349, 2016a.

900   Lyu, X. P., Guo, H., Simpson, I. J., Meinardi, S., Louie, P. K. K., Ling, Z. H., Wang, Y., Liu,

901   M., Luk, C. W. Y., Wang, N., and Blake, D. R.: Effectiveness of replacing catalytic

902   converters in LPG-fuelled vehicles in Hong Kong, Atmos. Chem. Phys., 16, 6609-6626,

903   2016b.

904   Lyu, X. P., Chen, N., Guo, H., Zhang,W. H., Wang, N.,Wang, Y., and Liu, M.: Ambient

905   volatile organic compounds and their effect on ozone production in Wuhan, Central China,

906   Sci. Total Environ., 541, 200-209, 2016c.

907   Lyu, X. P., Zeng, L. W., Guo, H., Simpson, I. J., Ling, Z. H., Wang, Y., Murray, F., Louie, P.

908   K. K., Saunders, S. M., Lam, S. H. M., and Blake, D. R.: Evaluation of the effectiveness of

909   air pollution control measure in Hong Kong, Environ. Pollut., 220, 87-94, 2017a.

910   Lyu, X. P., Guo, H., Wang, N., Simpson, I. J., Cheng, H. R., Zeng, L. W., Saunders, S. M.,

911   Lam, S. H. M., Meinardi, S., and Blake, D. R.: Modeling C_1-C_4 alkyl nitrate photochemistry

912   and their impacts on O_3 production in urban and suburban environments of Hong Kong, J.

913   Geophys. Res. Atmos., 122, 10539-10556, 2017b.

914   Madronich, S. and Flocke, S.: The role of solar radiation in atmospheric chemistry, Environ.

915   Photochem., 1-26, 1999.

916   Ministry of Ecology and Environment of the People's Republic of China (MEE PRC): Action

917   plan for preventing and controlling air pollution in Guangdong Province, China, available at:

918   http://www.mee.gov.cn/xxgk/hjyw/201403/t20140303_268619.shtml (last access: 25 October

919   2018), 2014.

920   NARSTO: An Assessment of tropospheric ozone pollution: a North American perspective,

921   NARSTO   synthesis   team,   available   at: http://cdiac.ess-dive.lbl.gov

922   /programs/NARSTO/ozone_assessment.html (last access: 25 October 2018), 2000.

923   National Research Council (NRC): Rethinking the ozone problem in urban and regional air

924   pollution, National Academies Press, 1992.

925   Norris, G., Wade, K., and Foley, C.: EPA Positive Matrix Factorization (PMF) 3.0

926   Fundamentals & User Guide, EPA 600/R-08/108, US Environmental Protection Agency,

927   Office of Research and Development, Washington, 2008.

928   Norris, G., Duvall, R., Brown, S., and Song, B.: EPA Positive Matrix Factorization (PMF)

929   5.0 Fundamentals & User Guide, EPA 600/R-14/108, US Environmental Protection Agency,

930   Office of Research and Development, Washington, 2014.

931   Ou, J.M., Guo, H., Zheng, J.Y., Cheung, K., Louie, P.K.K., Ling, Z.H., and Wang, D.W.:

932   Concentrations and sources of non-methane hydrocarbons (NMHCs) from 2005 to 2013 in

933   Hong Kong: A multi-year real-time data analysis. Atmos. Environ., 103, 196-206, 2015.

934   Paatero, P.: Least squares formulation of robust non-negative factor analysis, Chemometr.

935   Intell. Lab., 37, 23-35, 1997.

936   Paatero, P.: User's Guide for Positive Matrix Factorization Programs PMF2 and PMF3, Part

937   1: Tutorial, Prepared by University of Helsinki, Finland (February), 2000a.

938   Paatero, P.: User's Guide for Positive Matrix Factorization Programs PMF2 and PMF3, Part

939   2: Reference, Prepared by University of Helsinki, Finland, 2000b.

940 Parrish, D. D., Lamarque, J. F., Naik, V., Horowitz, L., Shindell, D. T., Staehelin, J., Derwent,

941 R., Cooper, O. R., Tanimoto, H., Volz-Thomas, A., and Gilge, S.: Long-term changes in

942 lower tropospheric baseline ozone concentrations: Comparing chemistry-climate models and

943 observations at northern midlatitudes., J. Geophys. Res. Atmos., 119, 5719-5736, 2014.

944 Polissar, A. V., Hopke, P. K., Paatero, P., Malm, W. C., and Sisler, J. F.: Atmospheric aerosol

945 over Alaska: 2. Elemental composition and sources, J. Geophys. Res. Atmos., 103, D15,

946 19045-19057, 1998.

947 Reff, A., Eberly, S. I., and Bhave, P. V.: Receptor modeling of ambient particulate matter

948 data using positive matrix factorization: review of existing methods, J. Air Waste Manag.

949 Assoc., 57, 146-154, 2007.

950 Richter, A., Burrows, J.P. Nub, H., Granier, C., and Niemeier, U.: Increase in tropospheric

951 nitrogen dioxide over China observed from space, Nature, 437, 129, 2005.

952 Sahoo, D., Petersen, B., and Miles, P.: Measurement of equivalence ratio in a light-duty low

953 temperature combustion diesel engine by planar laser induced fluorescence of a fuel tracer,

954 SAE Int. J. Engines, 4, 2312-2325, 2011.

955 Saunders, S. M., Jenkin, M. E., Derwent, R. G., and Pilling, M. J.: Protocol for the

956 development of the Master Chemical Mechanism, MCM v3 (Part A): tropospheric

957 degradation of non-aromatic volatile organic compounds, Atmos. Chem. Phys., 3, 161-180,

958 2003.

959 Schauer, J. J., Kleeman, M. J., Cass, G. R., and Simoneit, B. R.: Measurement of emissions

960 from air pollution sources. 2. C_1 through C_{30} organic compounds from medium duty diesel

961 trucks, Environ. Sci. Technol., 33, 1578-1587, 1999.

962 Sillman, S.: The relation between ozone, NO_x and hydrocarbons in urban and polluted rural

963 environments, Atmos. Environ., 33, 1821-1845, 1999.

964   Simpson, I. J., Blake, N. J., Barletta, B., Diskin, G. S., Fuelberg, H. E., Gorham, K., Huey, L.

965   G., Meinardi, S., Rowland, F. S., Vay, S. A., Weinheimer, A. J., Yang, M., and Blake, D. R.:

966   Characterization of trace gases measured over Alberta oil sands mining operations: 76

967   speciated C_2-C_{10} volatile organic compounds (VOCs), CO_2, CH_4, CO, NO, NO_2, NO_y, O_3 and

968   SO_2, Atmos. Chem. Phys., 10, 11931−11954, 2010.

969   So, K. L. and Wang, T.: On the local and regional influence on ground-level ozone

970   concentrations in Hong Kong, Environ. Pollut., 123, 307-317, 2003.

971   United States Environmental Protection Agency (US EPA): Positive Matrix Factorization

972   Model for environmental data analyses, available at https://www.epa.gov/air-

973   research/positive-matrix-factorization-model-environmental-data-analyses (last access: 25

974   October 2018), 2017.

975   Wang, H., Lyu, X. P., Guo, H., Wang, Y., Zou, S. C., Ling, Z. H., Wang, X. M., Jiang, F.,

976   Zeren, Y. Z., Pan, W. Z., Huang X. B., and Shen, J.: Ozone pollution around a coastal region

977   of South China Sea: Interaction between marine and continental air, Atmos. Chem. Phys., 18,

978   4277-4295, 2018b.

979   Wang, H. X., Kiang, C. S., Tang, X. Y., Zhou, X. J., and Chameides, W. L.: Surface ozone:

980   A likely threat to crops in Yangtze delta of China, Atmos. Environ., 39, 3843-3850, 2005.

981   Wang, N., Guo, H., Jiang, F., Ling, Z. H., and Wang, T.: Simulation of ozone formation at

982   different elevations in mountainous area of Hong Kong using WRF-CMAQ model, Sci. Total

983   Environ, 505, 939-951, 2015.

984   Wang, T., Wei, X. L., Ding, A. J., Poon, S. C., Lam, K. S., Li, Y. S., Chan, L. Y., and Anson,

985   M.: Increasing surface ozone concentrations in the background atmosphere of Southern China,

986   1994-2007, Atmos. Chem. Phys., 9, 6217-6227, 2009.

987 Wang, T., Xue, L. K., Brimblecombe, P., Lam, Y. F., Li, L., and Zhang, L.: Ozone pollution

988 in China: A review of concentrations, meteorological influences, chemical precursors, and

989 effects, Sci. Total Environ., 575, 1582-1596, 2017b.

990 Wang, Y., Wang, H., Guo, H., Lyu, X. P., Cheng, H. R., Ling, Z. L., Louie, P. K. K.,

991 Simpson, I J., Meinardi, S., and Blake, D. R.: Long-term O_3- precursor relationships in Hong

992 Kong: field observation and model simulation, Atmos. Chem. Phys., 17, 10919-10935, 2017a.

993 Wang, Y., Guo, H., Zou, S. C., Lyu, X. P., Ling, Z. H., Cheng, H. R., and Zeren, Y. Z.:

994 Surface O_3 photochemistry over the South China Sea: Application of a near-explicit chemical

995 mechanism box model, Environ. Pollut., 234, 155-166, 2018a.

996 Willmott, C. J.: Some comments on the evaluation of model performance., B. Am. Meteorol.

997 Soc., 63, 1309-1313, 1982.

998 Xu, X., Lin, W., Wang, T., Yan, P., Wang, J., Meng, Z., and Wang, Y.: Long-term trend of

999 surface ozone at a regional background station in eastern China 1991-2006: enhanced

1000 variability, Atmos. Chem. Phys., 8, 2595-2607, 2008.

1001 Xu, Z., Wang, T., Wu, J., Xue, L., Chan, J., Zha, Q., Zhou, S., Louie, P. K., and Luk, C. W.:

1002 Nitrous acid (HONO) in a polluted subtropical atmosphere: Seasonal variability, direct

1003 vehicle emissions and heterogeneous production at ground surface, Atmos. Environ., 106,

1004 100-109, 2015.

1005 Xue, L. K., Wang, T., Louie, P. K., Luk, C. W., Blake, D. R., and Xu, Z.: Increasing external

1006 effects negate local efforts to control ozone air pollution: a case study of Hong Kong and

1007 implications for other Chinese cities, Environ. Sci. Technol., 48, 10769-10775, 2014a.

1008 Xue, L. K., Wang, T., Gao, J., Ding, A. J., Zhou, X. H., Blake, D. R., Wang, X. F., Saunders,

1009 S. M., Fan, S. J., Zuo, H. C., and Zhang, Q. Z.: Ground-level ozone in four Chinese cities:

1010 precursors, regional transport and heterogeneous processes, Atmos. Chem. Phys., 14, 13175-

1011 13188, 2014b.

Xue, L. K., Gu, R. R., Wang, T., Wang, X. F., Saunders, S., Blake, D., Louie, P. K. K., Luk, C. W. Y., Simpson, I., Xu, Z., Wang, Z., Gao, Y., Lee, S. C., Mellouki, A., and Wang, W. X.: Oxidative capacity and radical chemistry in the polluted atmosphere of Hong Kong and Pearl River Delta regional analysis of a severe photochemical smog episode, Atmos. Chem., Phys., 16, 9891-9903, 2016.

Yao, C., Cheung, C. S., Cheng, C., Wang, Y., Chan, T. L., and Lee, S. C.: Effect of diesel/methanol compound combustion on diesel engine combustion and emissions, Energy Convers. Manag., 49, 1696-1704, 2008.

Yao, D., Lyu, X., Murray, F., Morawska, L., Yu, W., Wang, J., and Guo, H.: Continuous effectiveness of replacing catalytic converters on liquified petroleum gas-fueled vehicles in Hong Kong., Sci. Total Environ., 648, 830-838, 2019.

Zeng, L., Lyu, X., Guo, H., Zou, S., and Ling, Z.: Photochemical Formation of C_1–C_5 Alkyl Nitrates in Suburban Hong Kong and over the South China Sea, Environ. Sci. Technol., 52, 5581-5589, 2018.

Zhang, J., Wang, T., Chameides, W. L., Cardelino, C., Kwok, J., Blake, D. R., Ding, A., and So, K. L.: Ozone production and hydrocarbon reactivity in Hong Kong, Southern China, Atmos. Chem. Phys., 7, 557-573, 2007.

Zhang, Y., Wang, X., Blake, D.R., Li, L., Zhang, Z., Wang, S., Guo, H., Lee, S.C., Gao, B., Chan, L., and Wu, D.: Aromatic hydrocarbons as ozone precursors before and after outbreak of the 2008 financial crisis in the Pearl River Delta region, south China., J. Geophys. Res. Atmos., 117, D15306, https://doi.org/10.1029/2011JD017356, 2012.

Zheng, B., Tong, D., Li, M., Liu, F., Hong, C., Geng, G., Li, H., Li, X., Peng, L., Qi, J., and Yan, L.: Trends in China's anthropogenic emissions since 2010 as the consequence of clean air actions., Atmos. Chem. Phys., 18, 14095-14111, 2018.